

Dicke superradiance as nondestructive probe for the state of atoms in optical lattices

Nicolai ten Brinke^a and Ralf Schützhold^b

Fakultät für Physik, Universität Duisburg-Essen, Lotharstraße 1, D-47057 Duisburg, Germany

October 18, 2018

Abstract. We present a proposal for a probing scheme utilizing Dicke superradiance to obtain information about ultracold atoms in optical lattices. A probe photon is absorbed collectively by an ensemble of lattice atoms generating a Dicke state. The lattice dynamics (e.g., tunneling) affects the coherence properties of that Dicke state and thus alters the superradiant emission characteristics – which in turn provides insight into the lattice (dynamics). Comparing the Bose-Hubbard and the Fermi-Hubbard model, we find similar superradiance in the strongly interacting Mott insulator regime, but crucial differences in the weakly interacting (superfluid or metallic) phase. Furthermore, we study the possibility to detect whether a quantum phase transition between the two regimes can be considered adiabatic or a quantum quench.

1 Introduction

Optical lattices are artificial crystals of light, created by interfering optical laser beams [1]. Storing ultracold bosonic or fermionic atoms in optical lattices allows the creation of model systems in which many parameters can easily be controlled, including the periodic structure and the interaction between the atoms [1–4]. Remarkably, the virtual absence of decoherence and temperature effects in an isolated optical lattice enables a direct view on quantum many-body physics, thus rendering ultracold atoms in optical lattices a versatile tool [5] to be used in a wide range of experiments. One of the phenomena which can be studied particularly well is quantum phase transitions [6]. In the case of bosonic atoms in an optical lattice, for example, a phase transition between the superfluid phase, described by a macroscopic wave function spreading throughout the entire lattice, and the Mott insulator phase, corresponding to a fixed number of atoms per lattice site, is predicted by the Bose-Hubbard model [5, 7–9]. This phase transition, induced by varying the depth of the optical lattice potential, was observed experimentally [10–12] via time-of-flight measurements, in which the atoms are abruptly released from the lattice potential and their positions are then detected via absorption imaging. A matter-wave interference pattern featuring sharp peaks is obtained for the phase coherent superfluid state [10], while their absence indicates a Mott insulating state¹. Alternatively, the superfluid to Mott insulator transition was also detected via

microwave spectroscopy [14] or Bragg scattering [15]. In the case of fermions, on the other side, the Fermi-Hubbard model [5, 16] describes a metal-insulator transition, which has been extensively studied in the field of condensed-matter systems [17, 18]. While experimentally more challenging than in the case of bosons, the Fermi-Hubbard model was recently implemented in a three-dimensional optical lattice [19, 20]. In latest experiments, it was possible to detect metallic and insulating phases [21] and to observe the formation of a fermionic Mott insulator [22]. Notably, time-of-flight measurements directly image the Fermi surface of the atoms in the optical lattice, as initial momentum maps into final position [19, 20]. As opposed to measuring the momentum distribution of the lattice atoms, direct in situ imaging makes it possible to reconstruct the atom number distribution in the optical lattice with single-atom and single-site resolution, as realized in, e.g., [21, 23–27]. Although there is no doubt that the aforementioned methods offer extremely valuable insights, they suffer from an obvious drawback: the quantum state of the atoms in the optical lattice is destroyed or collapsed (loss of phase coherence) by the measurement. Therefore, other less destructive probing schemes were proposed, such as off-resonant collective light scattering from the atoms trapped in the optical lattice [28–31], described via a two-band Bose-Hubbard model coupled to cavity light fields [32–35]. Following this approach, measuring the light scattered into the optical cavity should allow to distinguish between different atomic quantum phases. For fermionic atoms in optical lattices, on the other hand, an all-optical pump-and-probe scheme to obtain information about dynamical (two-time) correlations was proposed recently [36]. Experimentally, vacuum-stimulated scattering of light was employed to nondestructive

^a e-mail: nicolai.ten-brinke@uni-due.de

^b e-mail: ralf.schuetzhold@uni-due.de

¹ This is a simplified view, however, as it was recently pointed out [13], that sharp peaks do not always pinpoint superfluidity.

tively measure the dynamic structure factor of a quantum gas [37]. Aside from light scattering, other approaches to nondestructively probe quantum phase transitions in an optical lattice are matter-wave scattering with (slow) atoms, as proposed in [38, 39], and the interference of the trapped atoms with a reference Bose-Einstein condensate [40].

In this paper, we extend the probing scheme first presented in [41] to a general formalism, placing special emphasis on the difference between bosonic and fermionic systems. We describe in detail an alternative, nondestructive detection method which is based on Dicke superradiance, i.e., the collective and coherent absorption and (time delayed) emission of photons from an ensemble of ultra-cold atoms [42–46]. To infer the quantum state of the optical lattice from the emission characteristics, we analyze in which way the lattice dynamics (e.g., tunneling), developing after the absorption of a single photon, alters its subsequent superradiant emission [47–50]. As opposed to the instantaneous off-resonant Bragg-type scattering into a cavity [28–31], we study resonant Dicke superradiance in free space with a time delay in between absorption and emission². Because of the time delay, our approach corresponds to pump-probe spectroscopy in analogy to solid state physics. Therefore, it provides important complementary information, e.g., for non-equilibrium phenomena. For instance, our method is sensitive to the correlator of creation and annihilation operators including their phase coherence at different times (see Eq. (11) below), as in e.g. [36, 40], instead of the correlator containing on-site number operators at the same time only, as in references [28–30].

Before we start with a detailed explanation of our model in the upcoming sections, let us briefly describe the general idea behind our probing scheme, as shown in Figure 1. The probing sequence consists of three steps. At first, the probe photon is sent almost (but not quite) orthogonally onto the two dimensional optical lattice, where it is absorbed by one of the lattice atoms. Assuming that the recoil of the probe photon is small enough such that it is transferred to the optical lattice, we cannot know which atom absorbed the photon. Thus, a coherent superposition state – a “timed” Dicke state [47–49] – is created. In a second step, the usual lattice dynamics (tunneling, interaction), as e.g. described by the Bose- or Fermi-Hubbard model, evolves during a waiting period Δt . Thirdly, the atoms collectively re-emit the previously absorbed probe photon. However, the tunneling of the lattice atoms altered the phase coherence of the Dicke state, thus resulting in modified emission characteristics, as compared to the

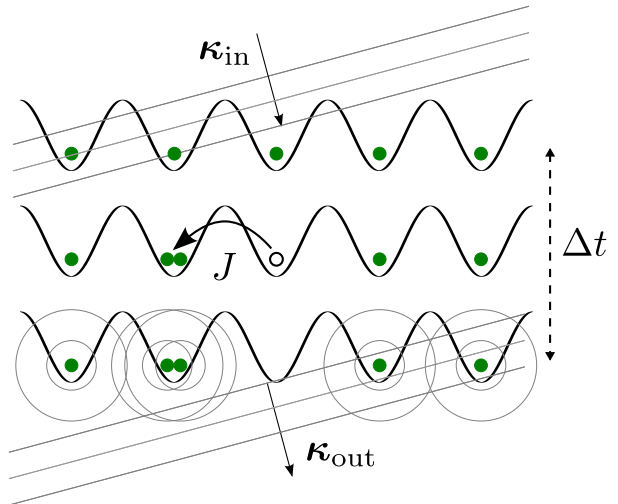


Fig. 1. Envisaged probing sequence: first, a probe photon κ_{in} is absorbed collectively by the ground-state atoms at their respective lattice sites. Second, the (bosonic or fermionic) atoms tunnel and interact according to, e.g., the Bose- or Fermi-Hubbard model during a waiting period Δt , thereby possibly compromising the spatial phase coherence of the Dicke state. In the third step, the probe photon is (collectively) emitted again with the wave vector κ_{out} – where the emission characteristics were probably altered due to the lattice dynamics.

case of immovable atoms. In this paper, we try to answer the question what can be learned about the quantum state (or about phase transitions) of the (bosonic or fermionic) optical lattice by observing these emission characteristics.

Next (Sect. 2), we introduce the basic model for our calculations, in particular, the Hamiltonians of the lattice dynamics and interaction with the probe photon, followed by a brief introduction to superradiance. In Section 3 we derive a general expression for the emission probability, which is then further investigated for different parameter regimes of the optical lattice in Section 4 (separable state) and Section 5 (weak interactions). The general findings are applied to concrete examples in terms of the Bose- and Fermi-Hubbard model, when we discuss which lattice states can be distinguished via our probing scheme in Section 6. Going further, we inspect what signs of quantum phase transitions can be detected by our probe in Section 7. We discuss several options for experimental realization in Section 8 and another particular option in Section 9, which employs classical laser fields instead of the absorption and spontaneous emission of a single photon. Finally, we conclude in Section 10.

2 Model

2.1 Hamiltonian

The basic idea of this paper is to investigate optical lattices via the interaction of the lattice atoms with infrared photons. Hence, we introduce the following general lattice Hamiltonian. It consists of a tunneling term with the

² We recently became aware of the pump-and-probe detection scheme presented in reference [36], which shares some key ingredients with our approach, e.g. the storage of a coherent light pulse, its decoherence due to lattice dynamics and its later retrieval which gives insight into the atomic two-time correlations. However, instead of focusing on fermions and the BCS superfluid state, we here develop a general method based on Dicke superradiance which can be applied to both bosonic and fermionic lattices in a variety of scenarios.

tunneling rate J and an on-site repulsion term with the interaction strength U ,

$$\hat{H}_{\text{lat}} = -\frac{J}{Z} \sum_{\mu\nu, s, \lambda} T_{\mu\nu} \hat{a}_{\mu s}^{\lambda\dagger} \hat{a}_{\nu s}^{\lambda} + \frac{U}{2} \sum_{\mu} \left(\sum_{s, \lambda} \hat{n}_{\mu s}^{\lambda} \right) \left(\sum_{s, \lambda} \hat{n}_{\mu s}^{\lambda} - 1 \right), \quad (1)$$

and describes the dynamics of cold atoms in an optical lattice, assuming lowest band occupation only and neglecting long-range interactions³. Furthermore, the adjacency matrix $T_{\mu\nu}$ and the coordination number Z are determined by the lattice structure. In our case, we assume a two-dimensional, quadratic lattice with $Z = \sum_{\nu} T_{\mu\nu} = 4$ and N lattice sites and atoms. Above all, $\hat{a}_{\mu s}^{\lambda\dagger}$ and $\hat{a}_{\nu s}^{\lambda}$ denote (bosonic or fermionic) creation and annihilation operators of atoms at lattice sites μ and ν , respectively. Their number operator is abbreviated as $\hat{n}_{\mu s}^{\lambda}$. In order to model the absorption and emission of photons by the atomic ensemble, we need to distinguish between (at least) two internal levels $\lambda \in \{\text{gr}, \text{ex}\}$ of the atoms. In addition, the index s refers to a potential extra spin quantum number – if applicable, such as for fermionic atoms. Note that we assume identical lattice dynamics (1) for both the ground and excited state atoms, for simplicity. However, our qualitative results do not depend on this presupposition⁴. The complete Hamiltonian of our system, including the general lattice dynamics as in equation (1) as well as the free-space electromagnetic field and the interaction between atoms and photons, is given by ($\hbar = 1$)

$$\hat{H} = \hat{H}_{\text{lat}} + \omega \sum_{\mu, s} \hat{n}_{\mu s}^{\text{ex}} + \int d^3k \omega_{\mathbf{k}} \hat{a}_{\mathbf{k}}^{\dagger} \hat{a}_{\mathbf{k}} + \hat{V}, \quad (2)$$

where the middle two terms account for the energy stored in the excited atoms (the energy gap between the two atomic levels is denoted by ω), and the energy stored in the electromagnetic field, respectively. Here, $\hat{a}_{\mathbf{k}}$ and $\hat{a}_{\mathbf{k}}^{\dagger}$ are the usual annihilation and creation operators for photons

with wave number \mathbf{k} . The internal states of the atoms are coupled to the electromagnetic field via the perturbation Hamiltonian in rotating-wave and dipole approximation,

$$\hat{V} = \int d^3k g_{\mathbf{k}}(t) \hat{a}_{\mathbf{k}} \hat{\Sigma}^+ (\mathbf{k}) + \text{H.c.}, \quad (3)$$

where the (time-dependent) coupling constant $g_{\mathbf{k}}(t)$ is assumed to be small. Note that it is not space-dependent as in e.g. [36], that is we assume equal coupling of all atoms. Most important, the exciton creation operator is given by:

$$\hat{\Sigma}^+ (\mathbf{k}) = \sum_{\mu, s} \hat{a}_{\mu s}^{\text{ex}\dagger} \hat{a}_{\mu s}^{\text{gr}} \exp \{ i \mathbf{k} \cdot \mathbf{r}_{\mu} \}, \quad (4)$$

where \mathbf{r}_{μ} is the position of the atom at the lattice site μ . Each summand describes the excitation of an (bosonic or fermionic) atom from the ground state to the excited state with the corresponding spatial phase factor. The sum over all lattice sites creates a (entangled, i.e., W-type) superposition state – in other words, we do not know which atom has been excited. Note that the spin quantum number s of the lattice atoms should not affect the hopping, interaction or excitation process, as considered via the summation over s in equations (1), (2) and (4).

2.2 Dicke superradiance

From the exciton creation operator $\hat{\Sigma}^+ (\mathbf{k})$ and its Hermitian conjugate counterpart, the exciton annihilation operator $\hat{\Sigma}^- (\mathbf{k}) = [\hat{\Sigma}^+ (\mathbf{k})]^{\dagger}$, quasispin- N -operators $\hat{\Sigma}^x (\mathbf{k})$, $\hat{\Sigma}^y (\mathbf{k})$ and $\hat{\Sigma}^z$ can be constructed via $\hat{\Sigma}^{\pm} (\mathbf{k}) = \hat{\Sigma}^x (\mathbf{k}) \pm i \hat{\Sigma}^y (\mathbf{k})$ and

$$\hat{\Sigma}^z = \frac{1}{2} [\hat{\Sigma}^+ (\mathbf{k}), \hat{\Sigma}^- (\mathbf{k})] = \frac{1}{2} \sum_{\mu, s} (\hat{n}_{\mu s}^{\text{ex}} - \hat{n}_{\mu s}^{\text{gr}}). \quad (5)$$

The quasispin- N -operators generate an $SU(2)$ algebra [44, 45], which leads to the astonishing effect that the transition probabilities roughly grow with the number N of atoms *times* the number n of excitations

$$\begin{aligned} \hat{\Sigma}^+ (\mathbf{k}) |n\rangle &= \sqrt{(N-n)(n+1)} |n+1\rangle, \\ \hat{\Sigma}^- (\mathbf{k}) |n\rangle &= \sqrt{(N-n+1)n} |n-1\rangle, \end{aligned} \quad (6)$$

where $|n\rangle \propto [\hat{\Sigma}^+ (\mathbf{k})]^n |0\rangle$ denotes a coherent superposition state with n excitons, often referred to as Dicke state [42]. Apart from the increased absorption and emission probability, another important consequence of the collective effects when an *ensemble* of atoms absorbs a photon is directed spontaneous emission [47–50]. In short, after the absorption of a photon with wave vector $\boldsymbol{\kappa}$, the atom-ensemble re-emits the photon predominantly in the same (forward) direction $\boldsymbol{\kappa}$. Intuitively speaking, the wave vector $\boldsymbol{\kappa}$ of the absorbed photon is remembered by the atom-ensemble via the spatial phases $\exp(i\boldsymbol{\kappa} \cdot \mathbf{r}_{\mu})$ in the Dicke state, stemming from exciton creation (4). In the following, we will restrict ourselves to *single-photon* superradiance, where according to equation (6), the absorption

³ Longer range (e.g. dipole-dipole) interactions are usually much weaker than the short range (on-site) forces, and are therefore neglected. Note that though ground and excited state atoms in general behave differently with regard to dipole-dipole interactions, the resulting phase factors would still be negligible in comparison with the phase factors stemming from the tunneling rate J , which are responsible for the effects discussed in this paper.

⁴ Although we assume that ground and excited state atoms underlie the same tunneling rate J and on-site repulsion U , the qualitative results of this paper hold true in the general case. In the separable state regime ($U \gg J$), for example, the important point is that the atoms are (almost) fixed to their lattice sites – which is also true for differing interaction strengths, as long as they are all large compared to the tunneling rate J . In the weak interactions regime ($J \gg U$), on the other hand, different J would appear in the formulae. But in the end, there are still the same distinguishable cases – either the usual superradiance or a decay of the superradiance peak.

($n = 0$) and directed spontaneous emission ($n = 1$) probabilities are enhanced by a factor N each.

However, certain requirements have to be met in order to reach superradiance. For instance, superradiant decay is dominant over incoherent emission processes when the lattice spacing ℓ of the optical lattice is small compared to the probe-photon wavelength λ [51]. Recent calculations and experiments [50, 52] suggest that it is sufficient when the lattice spacing is only slightly smaller (but still of the same order) than the driving wavelength. As another requirement, the atomic recoil due to the absorption or emission of the probe photon should be negligible. For both reasons, it is favorable to consider infrared photons. We will revisit this issue when discussing options for experimental realization in Section 8.

3 Emission Probability

In the formalism outlined above, let us now calculate the probability density for the event that a photon with wave vector κ_{in} is absorbed and subsequently re-emitted with wave vector κ_{out} after a waiting time Δt . Employing first-order perturbation theory for the absorption as well as for the emission process, the probability density reads

$$P = \left\| \langle 0 | \hat{a}_{\kappa_{\text{out}}} \int_0^{\tau_E} dt_2 \hat{V}(t_2) \int_0^{\tau_A} dt_1 \hat{V}(t_1) |\Psi\rangle \hat{a}_{\kappa_{\text{in}}}^\dagger |0\rangle \right\|^2. \quad (7)$$

Here, the $|0\rangle$ -ket refers to the vacuum state of the photon field, while $\hat{V}(t)$ denotes the perturbation Hamiltonian (3) in the interaction picture. The initial (bosonic or fermionic) state of the optical lattice $|\Psi\rangle$ can be arbitrary, except that we assume that there are no $\hat{a}_{\mu s}^{\text{ex}\dagger}$ -excitations in the beginning, i.e., $\hat{a}_{\mu s}^{\text{ex}} |\Psi\rangle = 0$ for all μ, s . Resolving the photon part yields an expression containing only the exciton creation operator (4) and its adjoint $(\hat{\Sigma}^+)^{\dagger} =: \hat{\Sigma}^-$ as operatorial part,

$$P = \mathcal{I} \left[e^{i(\omega_{\text{out}} t_2 - \omega_{\text{in}} t_1)} \hat{\Sigma}^-(\kappa_{\text{out}}, t_2) \hat{\Sigma}^+(\kappa_{\text{in}}, t_1) |\Psi\rangle \right], \quad (8)$$

where, in order to simplify notation, we introduced a functional $\mathcal{I}[f]$ as abbreviation

$$\mathcal{I}[f] = \left\| \int_0^{\tau_E} dt_2 \int_0^{\tau_A} dt_1 g_{\kappa_{\text{out}}}^*(t_2) g_{\kappa_{\text{in}}}(t_1) f(t_1, t_2) \right\|^2. \quad (9)$$

For further analysis of the operatorial part, we expand the probability density as a scalar product,

$$P = \int dt_1 dt_2 dt_3 dt_4 g_{\kappa_{\text{out}}}(t_4) g_{\kappa_{\text{out}}}^*(t_2) g_{\kappa_{\text{in}}}^*(t_3) g_{\kappa_{\text{in}}}(t_1) \times e^{i(\omega_{\text{in}} t_3 - \omega_{\text{out}} t_4)} e^{-i(\omega_{\text{in}} t_1 - \omega_{\text{out}} t_2)} \mathcal{D}(t_1, t_2, t_3, t_4), \quad (10)$$

and break it down to the individual lattice sites [41],

$$\begin{aligned} \mathcal{D}(t_1, t_2, t_3, t_4) = & \sum_{\mu\nu\rho\eta, s_1 s_2 s_3 s_4} \exp \{i(\kappa_{\text{out}} \cdot \mathbf{r}_\rho - \kappa_{\text{in}} \cdot \mathbf{r}_\eta)\} \\ & \times \exp \{-i(\kappa_{\text{out}} \cdot \mathbf{r}_\mu - \kappa_{\text{in}} \cdot \mathbf{r}_\nu)\} \\ & \times \langle \Psi | \hat{a}_{\eta s_4}^{\text{gr}\dagger}(t_3) \hat{a}_{\eta s_4}^{\text{ex}}(t_3) \hat{a}_{\rho s_3}^{\text{ex}\dagger}(t_4) \hat{a}_{\rho s_3}^{\text{gr}}(t_4) \\ & \times \hat{a}_{\mu s_1}^{\text{gr}\dagger}(t_2) \hat{a}_{\mu s_1}^{\text{ex}}(t_2) \hat{a}_{\nu s_2}^{\text{ex}\dagger}(t_1) \hat{a}_{\nu s_2}^{\text{gr}}(t_1) | \Psi \rangle. \quad (11) \end{aligned}$$

Note that while we presented the derivation for a pure state $|\Psi\rangle$ as the initial state of the optical lattice, we could as well start with an arbitrary mixed state $\hat{\rho}_{\text{in}}$, for example a thermal state, instead. In this case, the expectation value $\langle \Psi | \hat{A} | \Psi \rangle$ in the lower part of equation (11) is replaced by the corresponding expression for a mixed state, i.e., $\text{Tr}\{\hat{\rho}_{\text{in}} \hat{A}\}$. In any case, the lattice dynamics is incorporated in the operatorial function \mathcal{D} in equation (11) via the time-dependency of the annihilation and creation operators. In addition, the collective behavior of the absorption and emission is encoded in the summation of the spatial phases. In summary, all interesting phenomena are guided by the four-times eight-point function in the lower part of equation (11). Unfortunately, it cannot be solved explicitly for the general lattice Hamiltonian (1) without further assumptions. In the upcoming sections, we will thus study the limiting cases of separable states (i.e., small J) and weak interactions (i.e., $J \gg U$).

4 Separable state

Let us first have a look at the case of negligible correlations between the lattice sites. One example is the Mott insulator state (for $U \gg J$). Note that one should carefully distinguish correlations between lattice sites on the one hand from correlations between particles on the other hand. For example, the Mott insulator state is often called strongly correlated because it displays strong correlations between particles. However, the correlations between lattice sites become negligible for $U \gg J$.

We assume that the initial state $|\Psi\rangle$ can be written as a product of (bosonic or fermionic) normalized single-site states, i.e., we employ the Gutzwiller ansatz [53, 54],

$$|\Psi\rangle = \bigotimes_{\mu} |\Psi_{\mu}\rangle = \bigotimes_{\mu} (|\psi_{\mu}\rangle^{\text{gr}} \otimes |0_{\mu}\rangle^{\text{ex}}). \quad (12)$$

Obviously, there are zero correlations and no $\hat{a}_{\mu s}^{\text{ex}\dagger}$ -excitations at the beginning. Further, we set $t = t_{1/3}$ as the time at which the photon is absorbed and $t' = t_{2/4}$ as the time at which the photon is emitted again. This is justified, as we require that the waiting time $\Delta t = t' - t$ between the absorption and the emission of the photon is much larger than the time taken by the absorption or emission process itself, because the lattice dynamics is typically much slower. The correlator from (11) then reads

$$\begin{aligned} \mathcal{C}_{s_1 s_2 s_3 s_4}^{\mu\nu\rho\eta}(t, t') = & (\otimes_{\xi} \langle \Psi_{\xi} |) \hat{a}_{\eta s_4}^{\text{gr}\dagger}(t) \hat{a}_{\eta s_4}^{\text{ex}}(t) \hat{a}_{\rho s_3}^{\text{ex}\dagger}(t') \hat{a}_{\rho s_3}^{\text{gr}}(t') \\ & \times \hat{a}_{\mu s_1}^{\text{gr}\dagger}(t') \hat{a}_{\mu s_1}^{\text{ex}}(t') \hat{a}_{\nu s_2}^{\text{ex}\dagger}(t) \hat{a}_{\nu s_2}^{\text{gr}}(t) (\otimes_{\chi} | \Psi_{\chi} \rangle). \quad (13) \end{aligned}$$

Furthermore, we require that the correlations which arise during the waiting time Δt remain negligible. Under these assumptions, equation (13) can be evaluated for different cases regarding the indices. It turns out that to leading order in N , there is only one case where the correlator does not vanish (for details, see Appendix A),

$$\mathcal{C}_{s_1 s_2 s_3 s_4}^{\mu \eta \eta} (t, t') = \langle \Psi_\eta | \hat{a}_{\eta s_4}^{\text{gr} \dagger} (t) \hat{a}_{\eta s_4}^{\text{ex}} (t) \hat{a}_{\eta s_3}^{\text{ex} \dagger} (t') \hat{a}_{\eta s_3}^{\text{gr}} (t') | \Psi_\eta \rangle \\ \times \langle \Psi_\mu | \hat{a}_{\mu s_1}^{\text{gr} \dagger} (t') \hat{a}_{\mu s_1}^{\text{ex}} (t') \hat{a}_{\mu s_2}^{\text{ex} \dagger} (t) \hat{a}_{\mu s_2}^{\text{gr}} (t) | \Psi_\mu \rangle . \quad (14)$$

Inserting back into the operatorial part (11), and contracting the sums according to $\mu = \nu$ and $\eta = \rho$, the result can be written as an absolute square [41]

$$\mathcal{D}(t, t') = \left| \sum_{\mu, s_1 s_2} \exp \{ -i (\boldsymbol{\kappa}_{\text{out}} - \boldsymbol{\kappa}_{\text{in}}) \cdot \mathbf{r}_\mu \} \right. \\ \left. \times \langle \Psi_\mu | \hat{a}_{\mu s_1}^{\text{gr} \dagger} (t') \hat{a}_{\mu s_1}^{\text{ex}} (t') \hat{a}_{\mu s_2}^{\text{ex} \dagger} (t) \hat{a}_{\mu s_2}^{\text{gr}} (t) | \Psi_\mu \rangle \right|^2 . \quad (15)$$

The result for the operatorial function for separable states (15), is quite intuitive. It corresponds to the probability amplitude that the excited atom which is created at lattice site μ (with spin s_2) is still at the same position μ (with spin s_1) after the waiting time $\Delta t = t' - t$. Going to the extreme case of $J = 0$, i.e., the case of immovable atoms, the time-dependency of the creation and annihilation operators can be calculated explicitly and cancels out (up to a global temporal phase). Without $\hat{a}_{\mu s}^{\text{ex} \dagger}$ -excitations in $|\Psi_\mu\rangle$, the operatorial part (15) reduces to

$$\mathcal{D}(t, t') = \left| \sum_{\mu} \exp \{ -i (\boldsymbol{\kappa}_{\text{out}} - \boldsymbol{\kappa}_{\text{in}}) \cdot \mathbf{r}_\mu \} n_\mu \right|^2 , \quad (16)$$

where n_μ is just the total number of (ground-state) atoms at lattice site μ , i.e., $n_\mu = \sum_s \langle \Psi_\mu | \hat{n}_{\mu s}^{\text{gr}} | \Psi_\mu \rangle$. In other words, in the case $J = 0$, the sum can be understood as a discrete Fourier transform of the n_μ -distribution of the atoms in the optical lattice. An obvious example is a state with one atom per lattice site, $n_\mu = 1$, which yields a sharp peak $\mathcal{D}(t, t') = N^2 \delta_{\boldsymbol{\kappa}_{\text{in}} \boldsymbol{\kappa}_{\text{out}}}$ from the Fourier transform⁵. As in this case the atoms are fixed to their lattice sites, it is evident that we reproduce the well-known directed spontaneous superradiant emission [47–49],

$$P = N^2 \delta_{\boldsymbol{\kappa}_{\text{in}} \boldsymbol{\kappa}_{\text{out}}} P_{\text{single}} , \quad (17)$$

where P_{single} is the emission probability density for a single atom (for details, see Appendix B). Note that only one factor of N originates from the (single-photon) superradiant emission, while another factor N stems from the simple fact that N atoms absorb the incident probe photon more likely than one atom. However, keep in mind that (15) is only valid in the case of negligible correlations. Turning this argument around, a deviation from this behavior is then an indication for correlations. In Section 6 we will see clear deviations from equation (15).

⁵ Where we always use the atomic summation for a large number density, i.e., $\sum_{\mu} \exp \{ -i (\boldsymbol{\kappa}_{\text{out}} - \boldsymbol{\kappa}_{\text{in}}) \cdot \mathbf{r}_\mu \} = N \delta_{\boldsymbol{\kappa}_{\text{in}} \boldsymbol{\kappa}_{\text{out}}} .$

5 Weak interactions

Now we study the opposite limit, $J \gg U$, which typically features strong correlations between the lattice sites (think, e.g., of the superfluid state of the Bose-Hubbard model). Approximating $U = 0$, the general lattice Hamiltonian (1) becomes diagonal in the \mathbf{k} -basis (for further details, see Appendix C). Hence, the exciton creation operator (4) picks up a phase

$$\phi_{\mathbf{p}}^{\mathbf{k}}(t) = -J/Z(T_{\mathbf{p}} - T_{\mathbf{p}-\mathbf{k}})t , \quad (18)$$

in the interaction picture, i.e.⁶,

$$\hat{\Sigma}^+(\mathbf{k}, t) = e^{i\omega t} \sum_{\mathbf{p}, s} \hat{a}_{\mathbf{p}, s}^{\text{ex} \dagger} \hat{a}_{\mathbf{p}-\mathbf{k}, s}^{\text{gr}} \exp \{ i\phi_{\mathbf{p}}^{\mathbf{k}}(t) \} , \quad (19)$$

where $T_{\mathbf{p}}$ denotes the Fourier transform of the adjacency matrix $T_{\mu\nu}$. After inserting the exciton creation (19) and annihilation operator (its adjoint) into the probability density (8), we reduce the expression via $\hat{a}_{\mathbf{k}, s_1}^{\text{ex}} \hat{a}_{\mathbf{p}, s_2}^{\text{ex} \dagger} |\Psi\rangle = \delta_{\mathbf{k}\mathbf{p}} \delta_{s_1 s_2} |\Psi\rangle$, i.e., we employ (anti-)commutation relations and include the fact that $\hat{a}_{\mu s}^{\text{ex}} |\Psi\rangle = 0$. Moreover, we assume that the incoming photon is in resonance with the atomic transition, i.e., $\omega_{\text{in}} = \omega$. When we expand the probability density analogous to the lattice-site basis as in equations (10) and (11), we eventually find

$$P = \int dt_1 dt_2 dt_3 dt_4 g_{\boldsymbol{\kappa}_{\text{out}}}(t_4) g_{\boldsymbol{\kappa}_{\text{out}}}^*(t_2) g_{\boldsymbol{\kappa}_{\text{in}}}^*(t_3) g_{\boldsymbol{\kappa}_{\text{in}}}(t_1) \\ \times e^{-i(\omega_{\text{out}} - \omega)t_4} e^{i(\omega_{\text{out}} - \omega)t_2} \mathcal{E}(t_1, t_2, t_3, t_4) , \quad (20)$$

with the operatorial part \mathcal{E} , which once again contains the interesting phenomena,

$$\mathcal{E}(t_1, t_2, t_3, t_4) = \sum_{\mathbf{k}\mathbf{q}, s_1 s_2} \exp \{ i [\phi_{\mathbf{q}}^{\boldsymbol{\kappa}_{\text{out}}}(t_4) - \phi_{\mathbf{q}}^{\boldsymbol{\kappa}_{\text{in}}}(t_3)] \} \\ \times \exp \{ -i [\phi_{\mathbf{k}}^{\boldsymbol{\kappa}_{\text{out}}}(t_2) - \phi_{\mathbf{k}}^{\boldsymbol{\kappa}_{\text{in}}}(t_1)] \} \\ \times \langle \Psi | \hat{a}_{\mathbf{q}-\boldsymbol{\kappa}_{\text{in}}, s_2}^{\text{gr} \dagger} \hat{a}_{\mathbf{q}-\boldsymbol{\kappa}_{\text{out}}, s_2}^{\text{gr}} \hat{a}_{\mathbf{k}-\boldsymbol{\kappa}_{\text{out}}, s_1}^{\text{gr} \dagger} \hat{a}_{\mathbf{k}-\boldsymbol{\kappa}_{\text{in}}, s_1}^{\text{gr}} | \Psi \rangle . \quad (21)$$

Again, the result is also valid for a mixed state $\hat{\rho}_{\text{in}}$ instead of a pure state $|\Psi\rangle$ as the initial state of the optical lattice, when we substitute $\text{Tr}\{\hat{\rho}_{\text{in}} \hat{A}\}$ for the expectation value $\langle \Psi | \hat{A} | \Psi \rangle$. Note that so far, we did not specify whether we deal with bosonic or fermionic lattice atoms. However, as we will dive into two concrete examples in the upcoming Section 6 (namely the Bose- and Fermi-Hubbard model), we will differentiate between these two setups from now on. Regarding the four-point correlator in equation (21),

⁶ Please note that we tacitly required here that the wave vector \mathbf{k} is a lattice vector, and will continue to do so for any wave vector from now on. Otherwise, expressions would get quite lengthy and provide less insight, although our main results hold true. Here, for example, the μ -sum in (4) would not yield an exact Kronecker delta after the transformation to \mathbf{k} -space. However, in the experiment, the wave vector $\boldsymbol{\kappa}_{\text{in}}$ of the probe photon can simply be tuned such that it matches a lattice vector (Sect. 8).

we consider two cases in which it can be explicitly calculated.

First and foremost, if the initial pure state $|\Psi\rangle$ is diagonal in the \mathbf{k} -basis, we can define the eigenvalues of the number operator as $\hat{n}_{\mathbf{k},s}^{\text{gr}}|\Psi\rangle = n_s(\mathbf{k})|\Psi\rangle$, and express the four-point correlator in equation (21) in terms of these eigenvalues $n_s(\mathbf{k})$. In the case of bosons without spin quantum number (s_1, s_2 omitted), the correlator then yields

$$\begin{aligned} E_n^{\text{B}} &= \langle \Psi | \hat{a}_{\mathbf{q}-\boldsymbol{\kappa}_{\text{in}}}^{\text{gr}\dagger} \hat{a}_{\mathbf{q}-\boldsymbol{\kappa}_{\text{out}}}^{\text{gr}} \hat{a}_{\mathbf{k}-\boldsymbol{\kappa}_{\text{out}}}^{\text{gr}\dagger} \hat{a}_{\mathbf{k}-\boldsymbol{\kappa}_{\text{in}}}^{\text{gr}} | \Psi \rangle \\ &= n(\mathbf{k}-\boldsymbol{\kappa}_{\text{in}})n(\mathbf{q}-\boldsymbol{\kappa}_{\text{out}})(\delta_{\boldsymbol{\kappa}_{\text{in}}\boldsymbol{\kappa}_{\text{out}}} + \delta_{\mathbf{k}\mathbf{q}}) \\ &\quad + n(\mathbf{k}-\boldsymbol{\kappa}_{\text{in}})\delta_{\mathbf{k}\mathbf{q}} \\ &\quad - n(\mathbf{k}-\boldsymbol{\kappa}_{\text{in}})[n(\mathbf{q}-\boldsymbol{\kappa}_{\text{out}})+1]\delta_{\mathbf{k}\mathbf{q}}\delta_{\boldsymbol{\kappa}_{\text{in}}\boldsymbol{\kappa}_{\text{out}}}, \quad (22) \end{aligned}$$

while in the case of fermions with internal spin $s_1, s_2 \in \{\uparrow, \downarrow\}$, the correlator gives

$$\begin{aligned} E_n^{\text{F}} &= \langle \Psi | \hat{a}_{\mathbf{q}-\boldsymbol{\kappa}_{\text{in}},s_2}^{\text{gr}\dagger} \hat{a}_{\mathbf{q}-\boldsymbol{\kappa}_{\text{out}},s_2}^{\text{gr}} \hat{a}_{\mathbf{k}-\boldsymbol{\kappa}_{\text{out}},s_1}^{\text{gr}\dagger} \hat{a}_{\mathbf{k}-\boldsymbol{\kappa}_{\text{in}},s_1}^{\text{gr}} | \Psi \rangle \\ &= n_{s_1}(\mathbf{k}-\boldsymbol{\kappa}_{\text{in}})n_{s_2}(\mathbf{q}-\boldsymbol{\kappa}_{\text{out}})(\delta_{\boldsymbol{\kappa}_{\text{in}}\boldsymbol{\kappa}_{\text{out}}} - \delta_{\mathbf{k}\mathbf{q}}\delta_{s_1s_2}) \\ &\quad + n_{s_1}(\mathbf{k}-\boldsymbol{\kappa}_{\text{in}})\delta_{\mathbf{k}\mathbf{q}}\delta_{s_1s_2}. \quad (23) \end{aligned}$$

For details on the calculations, see Appendix D.

As an alternative, we can utilize Wick's theorem [55, 56] for Gaussian states $\hat{\rho}_{\text{g}}$, such as thermal states. Wick's theorem states that the four-point correlator in equation (21) can be expanded into a sum of products of two-point functions, when the Hamiltonian is quadratic in the annihilation and creation operators (which is the case for weak interactions, i.e., $U = 0$). The resulting two-point functions can then be expressed as the expectation values of the number operators in the Gaussian state, i.e., $n_s(\mathbf{k}) = \text{Tr}\{\hat{\rho}_{\text{g}}\hat{n}_{\mathbf{k},s}^{\text{gr}}\}$. After applying Wick's theorem, the result for the bosonic case is given by the first two lines of equation (22) – the last line does not appear in this case, as it corresponds to the situation where all four creation and annihilation operators act on the same \mathbf{k} -mode. Note that this discrepancy is insignificant, as the term in the last line is usually negligible compared to the first term. In the fermionic case, Wick's theorem yields the same expression (23) as for a diagonal pure state $|\Psi\rangle$.

We now have everything at hand to calculate the emission characteristics (7) via (20) in the limit of weak interactions ($J \gg U$) for a diagonal pure state $|\Psi\rangle$ or a Gaussian state $\hat{\rho}_{\text{g}}$. The remaining task is to insert the number distribution (in reciprocal space) $n_s(\mathbf{k})$ of the state, e.g., the number of particles per mode \mathbf{k} , in equation (22) or (23), respectively. Thus, in the next section, we will examine concrete lattice states in the context of the Bose- and Fermi-Hubbard model.

6 Probing lattice states

In this section, the general results above are applied to the two most commonly discussed optical lattice models – the Bose-Hubbard model and the Fermi-Hubbard model. To this end, a brief introduction on the respective model (and its ground states in different regimes) is given at the beginning of each subsection.

6.1 Bose-Hubbard model

On the one hand, bosonic ultracold atoms in optical lattices can approximately be described by the Bose-Hubbard Hamiltonian [5, 7–9]. The two-species Bose-Hubbard Hamiltonian is a special case of the general lattice Hamiltonian (1), describing the tunneling J and on-site repulsion U of bosons with no spin quantum number (i.e., index s omitted),

$$\begin{aligned} \hat{H}_{\text{BH}}^{2\text{sp}} &= -\frac{J}{Z} \sum_{\mu\nu,\lambda} T_{\mu\nu} \hat{b}_{\mu}^{\lambda\dagger} \hat{b}_{\nu}^{\lambda} \\ &\quad + \frac{U}{2} \sum_{\mu} \left(\sum_{\lambda} \hat{n}_{\mu}^{\lambda} \right) \left(\sum_{\lambda} \hat{n}_{\mu}^{\lambda} - 1 \right), \quad (24) \end{aligned}$$

where $\hat{b}_{\mu}^{\lambda\dagger}$ and \hat{b}_{ν}^{λ} are now *bosonic* creation and annihilation operators, of course. As we require that there are no excited bosons initially (and there is no way to excite them except the probe photon), the spectrum of possible initial lattice states is determined by the usual, single-species Bose-Hubbard Hamiltonian (i.e., index λ omitted),

$$\hat{H}_{\text{BH}} = -\frac{J}{Z} \sum_{\mu\nu} T_{\mu\nu} \hat{b}_{\mu}^{\dagger} \hat{b}_{\nu} + \frac{U}{2} \sum_{\mu} \hat{n}_{\mu}(\hat{n}_{\mu} - 1). \quad (25)$$

In the following, we will assume unit filling, $\langle \hat{n}_{\mu} \rangle = 1$, i.e., one boson per lattice site, on average. In this case, the Bose-Hubbard model features a quantum phase transition [6] between the Mott insulator state, where the interaction term dominates, $U \gg J$, and the superfluid phase, where the tunneling term dominates, $J \gg U$.

Mott insulator state In the first extremal limit, $U \gg J$, the atoms are pinned to their lattice sites and the ground state is given by the fully localized Mott insulator state,

$$|\Psi\rangle_{\text{Mo}}^{J=0} = \prod_{\mu} \hat{b}_{\mu}^{\dagger} |0\rangle = \bigotimes_{\mu} |1\rangle_{\mu}. \quad (26)$$

As discussed in Section 4, we obtain the usual single-photon superradiance in this case, i.e., the emission probability of the probe photon is enhanced by a factor N^2 as compared to the single atom case (17).

Superfluid ground state In the other extremal limit, $J \gg U$, the atoms can move freely across the entire lattice, which leads to the completely delocalized superfluid ground state,

$$|\Psi\rangle_{\text{sf}}^{U=0} = \frac{1}{\sqrt{N!}} (\hat{b}_{\mathbf{k}=0}^{\dagger})^N |0\rangle \propto \left(\sum_{\mu} \hat{b}_{\mu}^{\dagger} \right)^N |0\rangle. \quad (27)$$

In this case, the number distribution in Section 5 collapses to $n^{\text{sf}}(\mathbf{k}) = N\delta_{\mathbf{k}0}$, which yields for the bosonic four-point correlator (22)

$$E_{n^{\text{sf}}}^{\text{B}} = N(N-1)\delta_{\mathbf{k}\mathbf{q}\boldsymbol{\kappa}_{\text{in}}\boldsymbol{\kappa}_{\text{out}}} + N\delta_{\mathbf{k}\mathbf{q}\boldsymbol{\kappa}_{\text{in}}}. \quad (28)$$

When we insert this result into the operatorial part (21), all sums are fixed and we obtain a term proportional to N^2 to leading order. Its global phase $\exp\{i\phi_{\mathbf{k}_{\text{in}}}^{\text{in}}(t_4 - t_3 - t_2 + t_1)\}$ actually depends on the waiting time Δt (see Sect. 4), i.e., the time in between absorption and emission. As the waiting time Δt is assumed to be much larger than the timescales of the absorption and emission process itself, the phase can be regarded as constant over the integration periods. Thus we arrive at

$$P = N^2 \delta_{\mathbf{k}_{\text{in}} \mathbf{k}_{\text{out}}} P_{\text{single}} + \mathcal{O}(N), \quad (29)$$

where, again, P_{single} is the emission probability density for a single atom. Comparing (17) and (29), the two extremal bosonic ground states (26) and (27) show the same (single-photon) superradiant emission characteristics (to leading order in N), and are thus not distinguishable using our probe.

Partial condensation state Therefore we regarded a more general state in reference [41] which contains a certain number N_1 of bosons in the ground state at $\mathbf{k} = 0$ while the other N_2 bosons should be equally distributed between all \mathbf{k} -modes. Such a state could, for example, represent a simple toy model for a thermal state with partial condensation. Starting from the corresponding number distribution $n^{\text{dt}}(\mathbf{k}) = N_1 \delta_{\mathbf{k}0} + N_2/N$, we obtained the emission probability density (for a detailed derivation, see Appendix E)

$$P = \left| N_1 e^{i\varphi(\Delta t)} + N_2 \mathcal{J}(\Delta t) \right|^2 \delta_{\mathbf{k}_{\text{in}} \mathbf{k}_{\text{out}}} P_{\text{single}}. \quad (30)$$

Of course, for $N_1 = N$ and $N_2 = 0$, the result of the superfluid ground state (29) is reproduced. Much more interesting is the opposite scenario of a state where all \mathbf{k} -modes are equally populated by $N_2 > 0$ bosons. In this case, the emission probability decays over the waiting time Δt due to the phase-sum factor $\mathcal{J}(\Delta t)$ in equation (87) in Appendix E, except for an orthogonal probe photon with $\kappa_x = \kappa_y = 0$. The decay of the (single-photon) superradiance peak for $N_2 = N$ and $N_2 = N/2$ is shown in Figure 2 (dashed black lines). The dependence on the lattice vector becomes more clear when we approximate the phase-sum $\mathcal{J}(\Delta t)$ via Bessel functions J_0 , which is justified if the wave number is small compared to the lattice spacing $|\mathbf{k}|\ell \ll 1$, and the number of lattices sites in one dimension is large, $L \gg 1$ (see Appendix F),

$$\mathcal{J}(\Delta t) \approx J_0\left(2\frac{J\Delta t}{Z}\kappa_x\ell\right) J_0\left(2\frac{J\Delta t}{Z}\kappa_y\ell\right). \quad (31)$$

We find that the magnitude of the reduction is guided by $J\Delta t$, determining the amount of tunneling, times the wave-vector (components) $\kappa_{x/y}$. Qualitatively, this can be understood in the following picture. The decay of the superradiance peak is caused by the lattice dynamics during the waiting time Δt , in which the (excited) atoms tunnel according to the tunneling rate J and thus corrupt

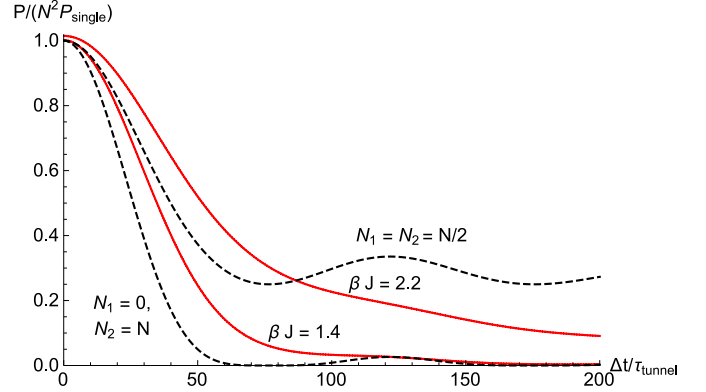


Fig. 2. Emission probability P from equation (20) (normalized by $N^2 P_{\text{single}}$, where one factor N originates from single-photon superradiance and another factor N stems from the absorption process) for emission in direction $\mathbf{k}_{\text{out}} = \mathbf{k}_{\text{in}} = 2\pi/(L\ell)\{1, 1\}$ over the waiting time Δt in units of the tunneling time $\tau_{\text{tunnel}} = \hbar/J$ for $N = L^2 = 100^2$ lattice sites and bosons. The dashed black lines represent numerical results for the partial condensation state (30), while the solid red lines represent numerical results for the Bose-Einstein distribution (32). Note that for high temperatures, $\beta J \ll 1$, the result for the Bose-Einstein distribution matches the result of the totally distributed case, as depicted by the lower dashed line.

the spatial phase coherence which is crucial for superradiance. A comparable effect – the reduction of superradiance due to motional effects – was recently observed experimentally for a dense coherent medium [50]. The damage inflicted on the phase coherence, however, also depends on how much the spatial phases of neighboring atoms differ – which is guided by the wave vector \mathbf{k} . In general, larger wave-vector components $\kappa_{x/y}$, i.e., a more skewed entrance angle of the probe photon, leads to a more rapid decay of the superradiance peak. In the extreme case of an orthogonal probe photon, $\kappa_x = \kappa_y = 0$, the spatial phases $\exp(i\mathbf{k} \cdot \mathbf{r}_\mu)$ do not differ at all and thus, there is no reduction. Note that the result (31) stands in opposition to the result we obtained for separable states (15), e.g., by its explicit dependence on the wave vector \mathbf{k} , thus demonstrating the importance of the correlations which arise due to the tunneling of the atoms.

Thermal state Instead of the above toy model state with partial condensation, let us now insert the more realistic Bose-Einstein distribution,

$$n^{\text{BE}}(\mathbf{k}) = \frac{1}{e^{\beta(E_{\mathbf{k}} - \mu)} - 1}, \quad (32)$$

where, according to the Bose-Hubbard model (75), the energy of a particle in the mode \mathbf{k} is given by $E_{\mathbf{k}} = -J/Z T_{\mathbf{k}}$ (for $U = 0$). In this case, the expressions (22) and (21) get quite lengthy, although they are still given analytically, of course. In particular, the phase-sums over \mathbf{k} and \mathbf{q} cannot be simplified, e.g., via Bessel-functions, as in the

partial condensation state (30). Thus, we show numerical results for the emission probability (20), where the Bose-Einstein distribution was inserted in equation (22), in Figure 2 (solid red lines).

Let us briefly sum up the results for a bosonic lattice. For the Mott state and the superfluid ground state, we obtained the usual single-photon superradiance – the result is independent of the waiting time Δt , implying the lattice dynamics in between absorption and emission does not change the emission characteristics. For (partially) excited states such as the toy-model state (30) or the more realistic Bose-Einstein distribution (32), the superradiance peak decays. In conclusion, bosonic (partially) excited states, such as, e.g., thermal states, can be distinguished from the superfluid ground state via Dicke superradiance.

6.2 Fermi-Hubbard model

On the other hand, fermionic ultracold atoms in optical lattices are approximately described by the Fermi-Hubbard Hamiltonian [5, 16]. The two-species Fermi-Hubbard Hamiltonian can be obtained from the general lattice Hamiltonian (1) by defining the possible spin states $s \in \{\uparrow, \downarrow\}$, and simplifying the on-site repulsion term for fermions,

$$\hat{H}_{\text{FH}}^{2\text{sp}} = -\frac{J}{Z} \sum_{\mu\nu, s, \lambda} T_{\mu\nu} \hat{c}_{\mu s}^\lambda \hat{c}_{\nu s}^\lambda + U \sum_{\mu} \left(\sum_{\lambda} \hat{n}_{\mu\uparrow}^\lambda \hat{n}_{\mu\downarrow}^\lambda + \sum_{s_1 s_2} \hat{n}_{\mu s_1}^{\text{gr}} \hat{n}_{\mu s_2}^{\text{ex}} \right). \quad (33)$$

Of course, $\hat{c}_{\mu s}^\lambda$ and $\hat{c}_{\nu s}^\lambda$ now denote *fermionic* creation and annihilation operators. To identify plausible initial states of the fermionic lattice, we explore the ground states of the single-species Fermi-Hubbard model, which describes the lattice dynamics prior to the absorption of the probe photon (i.e., index λ omitted),

$$\hat{H}_{\text{FH}} = -\frac{J}{Z} \sum_{\mu\nu, s} T_{\mu\nu} \hat{c}_{\mu s}^\dagger \hat{c}_{\nu s} + U \sum_{\mu} \hat{n}_{\mu\uparrow} \hat{n}_{\mu\downarrow}. \quad (34)$$

In the fermionic lattice, we consider the case of half-filling, with half of the atoms in the $s = \uparrow$ -state and half of the atoms in the $s = \downarrow$ -state, i.e., $\langle \hat{n}_{\mu\uparrow} \rangle = \langle \hat{n}_{\mu\downarrow} \rangle = 1/2$. Due to the Pauli exclusion principle, the analog of the superfluid state in the bosonic case is the metallic phase of the Fermi-Hubbard model.

Mott-Néel state In order to minimize the interaction energy, the ground state for $U \gg J$ has to be a state with one particle per lattice site, as in the bosonic case. Nevertheless, the ground state is highly degenerate for $J = 0$, as the energy is unchanged under local spin rotations. We will work with the Mott-Néel state, which is the approximate ground state for small but nonzero tunneling rate

J ,

$$|\Psi\rangle_{\text{Né}}^{J=0} = \prod_{\mu \in \mathcal{A}} \hat{c}_{\mu\uparrow}^\dagger \prod_{\nu \in \mathcal{B}} \hat{c}_{\nu\downarrow}^\dagger |0\rangle = \bigotimes_{\mu \in \mathcal{A}} |\uparrow\rangle_\mu \bigotimes_{\nu \in \mathcal{B}} |\downarrow\rangle_\nu. \quad (35)$$

To describe this state, we assume a bipartite lattice, i.e., we divide the total lattice into two sub-lattices \mathcal{A} and \mathcal{B} , where for each site $\mu \in \mathcal{A}$, all the neighboring sites ν belong to \mathcal{B} , and vice-versa. All the fermions at the lattice sites in \mathcal{A} have spin $s = \uparrow$ while all the fermions at the sites in \mathcal{B} have spin $s = \downarrow$, such that neighboring fermions always have opposite spin (checkerboard pattern). However, according to Section 4, we obtain the usual single-photon superradiance for all states with one atom per lattice site, irregardless of the spin. In other words, we get the same result for a fermionic lattice in the Mott-Néel state, as for the Mott insulator state in the case of a bosonic lattice.

Metallic ground state For the opposing case of $J \gg U$ and weak interactions, the particles arrange in the metallic ground state, which can be displayed in \mathbf{k} -space (Appendix C),

$$|\Psi\rangle_{\text{me}}^{U=0} = \prod_{E_{\mathbf{k}} < E_F, s} \hat{c}_{\mathbf{k}, s}^\dagger |0\rangle, \quad (36)$$

where the product goes over all \mathbf{k} -modes whose energy eigenvalues $E_{\mathbf{k}}$ are smaller than the Fermi energy E_F , and all spin orientations $s \in \{\uparrow, \downarrow\}$. In our configuration of a fermionic 2D-lattice with half-filling and the dispersion relation of the Fermi-Hubbard model (75), $E_{\mathbf{k}} = -J/Z T_{\mathbf{k}}$ with $T_{\mathbf{k}} = 2 [\cos(k_x \ell) + \cos(k_y \ell)]$ (for $U = 0$), the occupied modes form a diamond in two-dimensional \mathbf{k} -space whose vertices touch the borders of the first Brillouin zone, i.e., a $(\pi/\ell \times \pi/\ell)$ square rotated by $\pi/4$ [57]. Accordingly, the distribution function in Section 5 is approximately⁷ given by:

$$n_s^{\text{me}}(\mathbf{k}) = \begin{cases} 1, & \text{if } |k_x| + |k_y| < \pi/\ell, \\ 0, & \text{otherwise.} \end{cases} \quad (37)$$

We obtain the emission probability for the metallic ground state by inserting $n_s^{\text{me}}(\mathbf{k})$ into equation (23) and further into equations (21) and (20). It turns out (see Fig. 3) that a decay of the (single-photon) superradiance peak similar to the bosonic distributed case (30 with $N_1 = 0$ and $N_2 = N$) occurs (recall the lower dashed line in Fig. 2). The similarity is quite intuitive, since in both cases many different \mathbf{k} -modes are involved in the absorption and re-emission of the probe photon – all \mathbf{k} -modes in the bosonic

⁷ In a finite lattice with $N = L^2$ lattice sites (where L is even) and exactly N (fermionic) atoms, the metallic ground state is degenerate, as the edge of the diamond has $4(L-1)$ \mathbf{k} -modes with the same energy eigenvalue $E_{\mathbf{k}}$, but there are only $2(L-1)$ atoms left to fill these modes. Thus, we use the distribution function (37), describing the exact metallic ground state for a modified number of $N - 2(L-1) \approx N$ atoms, as a (for $L \gg 1$) very good approximation.

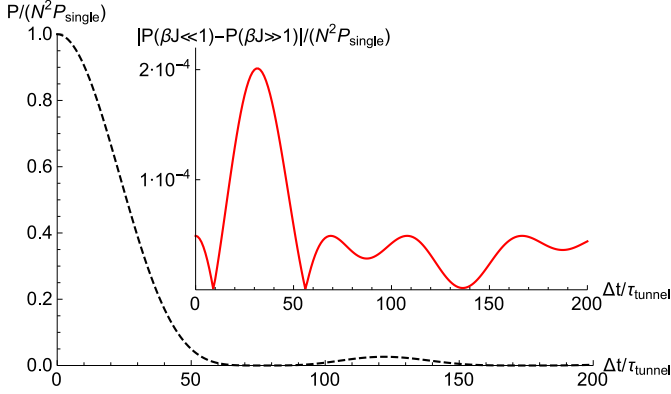


Fig. 3. Emission probability P from equation (20) (normalized by $N^2 P_{\text{single}}$, where one factor N originates from single-photon superradiance and another factor N stems from the absorption process) for emission in direction $\kappa_{\text{out}} = \kappa_{\text{in}} = 2\pi/(L\ell) \{1, 1\}$ over the waiting time Δt in units of the tunneling time $\tau_{\text{tunnel}} = \hbar/J$ for $N = L^2 = 100^2$ lattice sites and fermions. The dashed black line represents the numerical results for the metallic ground state (38). For small κ , the decay of the superradiance peak is identical to the bosonic distributed case (lower dashed line in Fig. 2). As the Fermi-Dirac distribution only interpolates between these two states with the same emissive behavior, the decay is similar for arbitrary temperatures βJ – aside from the minuscule deviations shown in the inset (solid red line).

case and half of them (the diamond) in the fermionic case – instead of just one mode, as in the bosonic superfluid ground state. For small wave numbers $|\kappa|\ell \ll 1$, as we suppose in the numerical and experimental examples, it can be shown analytically that the fermionic metallic ground state (36) gives the same emission probability,

$$P = N^2 |\mathcal{J}(\Delta t)|^2 \delta_{\kappa_{\text{in}} \kappa_{\text{out}}} P_{\text{single}}, \quad (38)$$

as the bosonic distributed case, i.e., with the sum over all \mathbf{k} -modes, which can be approximated via Bessel functions (31). The reason can be found in the phase-sum as in Appendix F. Imagine shifting the diamond by e.g. $\Delta \mathbf{k} = \pi/\ell \{1, 1\}$, i.e., into the empty regions of the first Brillouin zone. Doing so, only the sign of the sine-function in equation (93) changes, which is irrelevant with respect to the symmetric summation.

Thermal state For nonzero temperatures, one can insert the Fermi-Dirac distribution,

$$n^{\text{FD}}(\mathbf{k}) = \frac{1}{e^{\beta(E_{\mathbf{k}} - \mu)} + 1}, \quad (39)$$

into equation (23). Numerical results for the emission probability for arbitrary temperatures βJ are hardly different from the result for the metallic ground state, however (i.e., the deviations are always smaller than shown in the inset in Fig. 3). This becomes clear when considering that the

Fermi-Dirac distribution does nothing else than to interpolate between the metallic ground state (low temperature, $\beta J \gg 1$), and the totally distributed case (high temperature, $\beta J \ll 1$), where each \mathbf{k} -mode is populated by one atom. As we have just shown that (for small κ) these both extreme ends of the temperature scale show the same analytic result (38), it is clear that interpolating between these two extremes does not produce qualitatively different results.

In conclusion for a fermionic lattice, we obtained the usual single-photon superradiance only for the Mott-Néel state (Sect. 4). The metallic ground state as well as (partially) excited states show a reduction in superradiance. Thus, as opposed to the bosonic case, fermionic (partially) excited states cannot be distinguished from the metallic ground state in the weak interactions regime. However, in the fermionic case, the Mott-Néel state can be distinguished from the metallic ground state, i.e., the current parameter regime ($J \gg U$ or $U \gg J$) can be detected using our probe.

7 Phase transitions

In the previous sections, we discussed to what extent the proposed probe can be used to (nondestructively) detect certain lattice states in either of the limiting cases. As another application, we will now discuss the probe of a quantum phase transition from the separable state regime (small J) to the weak interactions regime ($J \gg U$). To this end, we consider a similar probing sequence as in Figure 1. First, the probe photon κ_{in} is absorbed by the bosonic or fermionic lattice, which is initially in the Mott insulator state (26) or the Mott-Néel state (35), respectively. Afterwards, either a sudden quantum quench or an adiabatic transition to the weak interactions regime is applied. Then, the sequence continues as before – after a waiting period Δt , in which the atoms have time to tunnel and interact, the probe photon is re-emitted.

Analogous to equation (7), we consider the absorption of the probe photon in first order perturbation theory, leading to the (non-normalized) excited state

$$|\Psi\rangle_{\text{ex}}^{\text{Mo/Né}} = -i \int_0^{\tau_A} dt_1 \hat{V}_U(t_1) |\Psi\rangle_{\text{Mo/Né}}^{J=0} \hat{a}_{\kappa_{\text{in}}}^\dagger |0\rangle, \quad (40)$$

where the index U of the perturbation Hamiltonian denotes that only interaction applies, as we are in the separable state regime ($J = 0$) in the beginning. In addition, the superscript Mo indicates the bosonic Mott insulator state (26), while Né is an abbreviation for the fermionic Mott-Néel state (35). As suggested by the diagonal slash, we consider both cases simultaneously where possible.

7.1 Sudden quantum quench

In the case of a sudden quantum quench, the initial excited state (40) cannot adapt adiabatically and is thus not an

eigenstate of the new ($U = 0$) Hamiltonian. We now calculate the emission probability density after such a sudden transition, i.e., starting from the excited Mott insulator state or the excited Mott-Néel state (40). Applying first order perturbation theory for the emission process (the index J denotes that only tunneling applies, as we are in the weak interactions regime, $U = 0$, after the transition),

$$P = \left\| \langle 0 | \hat{a}_{\mathbf{\kappa}_{\text{out}}} \int_0^{\tau_E} dt_2 \hat{V}_J(t_2) | \Psi \rangle_{\text{ex}}^{\text{Mo/Né}} \right\|^2, \quad (41)$$

we obtain an expression analog to equation (8). For convenience, we insert both the exciton creation operator and the exciton annihilation operator in the \mathbf{k} -basis (as in Sect. 5). However, as we are still in the separable state ($J = 0$) regime during exciton creation $\hat{\Sigma}_U^+(\mathbf{\kappa}_{\text{in}}, t_1)$, its phase factor (18) does not emerge here,

$$\begin{aligned} \hat{\Sigma}_J^-(\mathbf{\kappa}_{\text{out}}, t_2) \hat{\Sigma}_U^+(\mathbf{\kappa}_{\text{in}}, t_1) | \Psi \rangle_{\text{Mo/Né}}^{J=0} &= e^{i\omega(t_1-t_2)} \\ &\times \sum_{\mathbf{k}, s} \exp \{ -i\phi_{\mathbf{k}}^{\mathbf{\kappa}_{\text{out}}} (t_2) \} \hat{a}_{\mathbf{k}-\mathbf{\kappa}_{\text{out}}, s}^{\text{gr} \dagger} \hat{a}_{\mathbf{k}-\mathbf{\kappa}_{\text{in}}, s}^{\text{gr}} | \Psi \rangle_{\text{Mo/Né}}^{J=0}. \end{aligned} \quad (42)$$

Accordingly, the same four-point correlator as in equation (21) has to be calculated – but now the expectation value has to be taken in the Mott state (26) or the Mott-Néel state (35), respectively. The bosonic correlator as in equation (22), taken in the Mott insulator state $| \Psi \rangle_{\text{Mo}}^{J=0}$, yields

$$E_{\text{Mo}}^{\text{B}} = \delta_{\mathbf{\kappa}_{\text{in}} \mathbf{\kappa}_{\text{out}}} + 2\delta_{\mathbf{k} \mathbf{q}} - 2/N, \quad (43)$$

while the fermionic correlator as in (23), taken in the Mott-Néel state $| \Psi \rangle_{\text{Né}}^{J=0}$, gives

$$\sum_{s_1 s_2} E_{\text{Né}}^{\text{F}} = \delta_{\mathbf{\kappa}_{\text{in}} \mathbf{\kappa}_{\text{out}}} + \delta_{\mathbf{k} \mathbf{q}}/2. \quad (44)$$

For details on the calculation, see Appendix G. As in the derivation in Appendix E, we only keep the terms which contribute quadratically in N to the emission probability density (41), i.e., the leading order terms which correspond to coherent (single-photon) superradiant emission, as indicated by the factor $\delta_{\mathbf{\kappa}_{\text{in}} \mathbf{\kappa}_{\text{out}}}$. The resulting emission probability density (41) in the same direction in which the absorbed photon was incoming, $\mathbf{\kappa} = \mathbf{\kappa}_{\text{in}} = \mathbf{\kappa}_{\text{out}}$, is thus given by

$$P = N^2 \delta_{\mathbf{\kappa}_{\text{in}} \mathbf{\kappa}_{\text{out}}} \mathcal{I} \left[e^{i(\omega_{\text{out}} - \omega)t_2} \mathcal{J}(t_2) \right]. \quad (45)$$

So far, we did not account for the waiting time Δt . Here, we model it via the time-dependent coupling constant $g_{\mathbf{\kappa}_{\text{out}}}^*(t_2)$ in equation (9), which should be zero for a period Δt after the sudden transition and before the emission process starts as usual, e.g.,

$$g_{\mathbf{\kappa}_{\text{out}}}^*(t_2) = \begin{cases} 0, & \text{if } t_2 < \Delta t, \\ g_{\mathbf{\kappa}_{\text{out}}}^*, & \text{if } t_2 \geq \Delta t. \end{cases} \quad (46)$$

As the time span of the emission process is negligible in comparison to the waiting time Δt , we can approximate $\mathcal{J}(t_2) = \mathcal{J}(\Delta t)$ and thus arrive at

$$P = N^2 |\mathcal{J}(\Delta t)|^2 \delta_{\mathbf{\kappa}_{\text{in}} \mathbf{\kappa}_{\text{out}}} P_{\text{single}}. \quad (47)$$

That is, the emission probability after a sudden switching procedure shows a reduction in superradiance similar to the bosonic distributed case (30 with $N_1 = 0$ and $N_2 = N$) and the fermionic metallic ground state (38). The result is quite intuitive – after the sudden switch, the Mott (or Mott-Néel) state behaves as a state where all momenta are equally populated, as it appears as a mixture of excited states to the new ($U = 0$) Hamiltonian.

7.2 Adiabatic transition

In contrast to a quantum quench, i.e., an abrupt change of the parameter regime, let us now consider an adiabatic transition, i.e., a very slow change of the parameter in a finite lattice – such that the system stays close to its instantaneous ground (or excited) state. The case of a bosonic lattice was already studied in reference [41], where we came to the conclusion that the superradiance peak does not decay after an adiabatic transition, i.e., the superradiant emission probability reads $P = N^2 \delta_{\mathbf{\kappa}_{\text{in}} \mathbf{\kappa}_{\text{out}}} P_{\text{single}}$. For a detailed derivation of this result, see Appendix H.

Summing up for a bosonic lattice, the (single-photon) superradiance peak thus decays according to equation (47) after a sudden quantum quench, while it does not decay in the case of an adiabatic transition. Hence, employing the proposed probing scheme, a sudden transition can be distinguished from an adiabatic transition via the different emission characteristics.

Let us now study the fermionic case, which will yield a different result. In principal, starting from equation (40), the same reasoning as in the bosonic case applies. Anyway, in the case of fermions, we cannot unambiguously identify the corresponding eigenstate in the weak interactions regime. Taking, e.g., the metallic ground state (36) as a reasonable starting point, it is not clear which of the various \mathbf{k} -modes would carry the exciton wave number $\mathbf{\kappa}_{\text{in}}$ – whereas in the bosonic case there is obviously only one possibility. However, a first approximation for small wave vectors $\mathbf{\kappa}$ can be obtained by considering the commutator between the (time-dependent) Hamiltonian $\hat{H}_A(t)$ modeling the adiabatic evolution and the exciton creation operator, $\hat{\Sigma}_U^+(\mathbf{\kappa}_{\text{in}}, t_1)$,

$$\begin{aligned} \left[\hat{H}_A(t), \hat{\Sigma}_U^+(\mathbf{\kappa}_{\text{in}}, t_1) \right] &= -\frac{J(t)}{\mathcal{Z}} e^{i\omega t_1} \\ &\times \sum_{\mathbf{p}, s} \hat{c}_{\mathbf{p}-\mathbf{\kappa}_{\text{in}}, s}^{\text{gr}} \hat{c}_{\mathbf{p}, s}^{\text{ex} \dagger} (T_{\mathbf{p}} - T_{\mathbf{p}-\mathbf{\kappa}_{\text{in}}}). \end{aligned} \quad (48)$$

Notably, the commutator scales linearly in $(\mathbf{\kappa}_{\text{in}})_{x/y}$ for small wave vectors $|\mathbf{\kappa}_{\text{in}}| \ll 1$, see (91) in Appendix F. Presuming that the commutator is negligible, we can apply the adiabatic evolution $\hat{U}_A(t) | \Psi \rangle_{\text{Né}}^{J=0} = | \Psi \rangle_{\text{me}}^{U=0}$ before

the exciton creation operator instead of afterwards. Then, however, the emission probability (41) can be calculated via

$$\hat{\Sigma}_J^-(\boldsymbol{\kappa}_{\text{out}}, t_2) \hat{\Sigma}_U^+(\boldsymbol{\kappa}_{\text{in}}, t_1) |\Psi\rangle_{\text{me}}^{U=0} = e^{i\omega(t_1-t_2)} \times \sum_{\mathbf{k}, s} \exp\{-i\phi_{\mathbf{k}}^{\boldsymbol{\kappa}_{\text{out}}}(t_2)\} \hat{c}_{\mathbf{k}-\boldsymbol{\kappa}_{\text{out}}, s}^{\text{gr}\dagger} \hat{c}_{\mathbf{k}-\boldsymbol{\kappa}_{\text{in}}, s}^{\text{gr}} |\Psi\rangle_{\text{me}}^{U=0}, \quad (49)$$

which traces back to the case of the metallic ground state, for which we already showed that the superradiance peak decays as (38), i.e.,

$$P = N^2 |\mathcal{J}(\Delta t)|^2 \delta_{\boldsymbol{\kappa}_{\text{in}} \boldsymbol{\kappa}_{\text{out}}} P_{\text{single}}. \quad (50)$$

Even in the general case, where the adiabatic evolution does not commute with exciton creation, the quantum state after the adiabatic evolution has to be found somewhere in the spectrum between the metallic ground state and a thermal state. As we have shown in Section 6.2 and is particularly clear in Figure 3, both ends of this spectrum show the same reduction in superradiance (50). So in conclusion for a fermionic lattice, we expect a decay of the superradiance peak after a sudden quantum quench as well as after an adiabatic evolution. Thus, unfortunately, and in contrast to the phase transition in the bosonic lattice, we cannot distinguish a sudden transition from an adiabatic transition in a fermionic lattice.

8 Experimental realization

After having developed the theoretical framework of our probing scheme both for probing the quantum state of an optical lattice (Sect. 6), as well as properties of phase transitions (Sect. 7), we want to discuss the overall parameters for experimental implementation. As mentioned in Section 2, it is desirable that the probe-photon wavelength λ_{photon} is large compared to the lattice spacing $\ell = \lambda_{\text{lat}}/2$. Thus, ideally, one would like to have a small lattice spacing, e.g., a green lattice $\ell = 257 \text{ nm}$ [5, 8, 58] created by an argon-ion [59] laser with $\lambda_{\text{lat}} = 514 \text{ nm}$. On the other side, using an infrared probe photon with a wavelength of $\lambda_{\text{photon}} = 2\pi/|\boldsymbol{\kappa}_{\text{in}}| = 10.6 \mu\text{m}$ [60], then makes sure that the collective coherent emission (i.e., Dicke superradiance) outpaces spontaneous incoherent emission processes by a wide margin [51]. Moreover, the atomic recoil is negligible in case of an infrared photon, as its recoil energy is a factor $E_R^{\text{lat}}/E_R^{\text{photon}} = 4 \cdot 10^2$ smaller than the recoil energy of an optical lattice photon. This specific combination of trapping atoms (or molecules) which feature a far-infrared transition in a green lattice may be difficult to achieve experimentally. However, recent calculations and experiments [50, 52] suggest that cooperative effects still dominate even when the lattice spacing ℓ is only slightly smaller (but still of the same order) than the driving wavelength λ_{photon} . Hence, on the one hand, it should also be feasible to use larger optical lattice wavelengths, e.g., in the common range $\lambda_{\text{lat}} = 500 - 1000 \text{ nm}$ [10, 19, 22, 61–63], which is beneficial as the lattice wavelength can then be chosen to

fit the properties of the trapped atoms. On the other hand, a smaller optical wavelength, e.g., in the near-infrared, $\lambda_{\text{photon}} = 1 - 10 \mu\text{m}$, should also be possible. As for the required number of atoms, we envisage it in the typical range of 2D optical lattice experiments [12, 23, 25–27], i.e., in the range of $N = 10^2 - 10^4$ atoms and lattice sites. Of course, the higher the number of involved atoms, the stronger is the utilized effect of single-photon superradiance which leads to an increased sensitivity of the proposed probe. On the other hand, it becomes harder to fulfill the assumption of equal coupling (3). Below, we reflect on four possible setups for experimental realization (including the next Sect. 9).

8.1 Two-level system

The probing sequence displayed in Figure 1 basically poses two requirements on the physical system. First and foremost, the atoms in the optical lattice need to support an infrared transition via their level scheme, in order to be able to absorb and re-emit the infrared probe photon. Second, the lifetime of this transition needs to be long as compared to the time scales of the lattices dynamics, i.e., (much) longer than the typical tunneling time of $\tau_{\text{tunnel}} = \hbar/J = 5 \cdot 10^{-5} \text{ s}$, such that significant tunneling can occur before the re-emission. Hence, two-level atoms with a corresponding level scheme would suffice to implement the probing sequence. Although in principle the scheme could be implemented via a simple two-level system, the requirements are probably hard to meet when focusing on the atoms typically used in optical lattice experiments (e.g., Rb, Na). However, choosing different atoms (elements) or even considering molecules [62, 63] may render a direct implementation possible.

8.2 Assisted multi-photon transition

In order to overcome the requirement on the transition lifetime and, in addition, gain full experimental control over the waiting time Δt , one can replace the single-photon transition envisaged above by a laser-assisted multi-photon transition. In this scenario, the infrared transition of the probe photon is enabled only while the assisting lasers are switched on. Thus, switching the lasers on for the absorption and emission of the infrared probe photon, but switching them off for an arbitrary waiting time Δt in between, leaves the control of the involved time scales at the discretion of the experimentalist. Note that then also long waiting times of, e.g., $\Delta t = \mathcal{O}(10^2) \cdot \tau_{\text{tunnel}}$ are feasible, preferable to best distinguish different states or phase transitions (see, e.g., Fig. 2). An example of a detuned four-photon transition is presented in Figure 4a. Here, the four-photon transition involving the absorption or emission of an infrared probe photon γ_{IR} is assisted by three photons γ_1 , γ_2 , and γ_4 , which are provided by the assisting external lasers. Note that the four-photon transition as depicted in Figure 4a only serves as an example – the assisting lasers can be chosen as to match a wide variety of given level schemes.

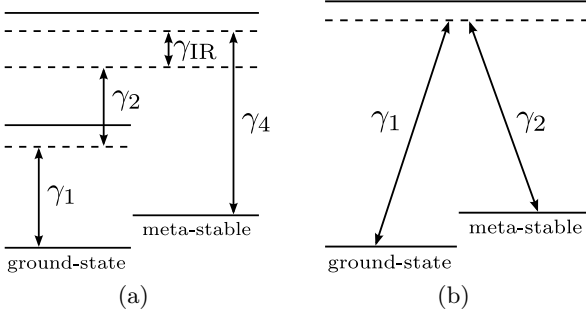


Fig. 4. Two examples of level schemes proposed for the experimental implementation. (a) In a detuned four-photon transition, the infrared probe photon γ_{IR} can only be absorbed or emitted under assistance of the laser fields γ_1 , γ_2 , and γ_4 . (b) Detuned two-photon Raman transition. Excitation either via a single photon γ_1 (where a Stokes photon γ_2 is scattered), or via two counter-propagating lasers γ_1 and γ_2 .

8.3 Two-photon Raman process

One can also think of a two-photon Stokes Raman scattering process to create the Dicke state among the optical lattice atoms, see, e.g., [47, 48]. For example, consider the level scheme shown in Figure 4b. An incident photon γ_1 leads to an excitation of the metastable level via the scattering of a Stokes photon γ_2 with wave vector \mathbf{k}_2 . The excitation vector $\mathbf{\kappa}_{\text{in}}$ of the created Dicke state can then be determined by detecting the Stokes photon, i.e., $\mathbf{\kappa}_{\text{in}} = \mathbf{k}_1 - \mathbf{k}_2$, and should be in the infrared region. Analogously, the emission process would correspond to an anti-Stokes Raman scattering, initiated by a suitable pulse on demand.

9 Classical laser fields

As a fourth option, we would like to present an alternative probing scheme, employing coherent states as generated by classical laser fields, instead of single-photon absorption and emission. While working with classical laser fields may be experimentally less challenging than the absorption and emission of single photons, we will show that main results of our probing scheme are retained, although the excitation (and deexcitation) dynamics differ. Basically, we again consider the two-photon (Raman) transition as given in Figure 4b, but this time operated via two counter-propagating lasers γ_1 and γ_2 . We envisage the following modified sequence. First, two counter-propagating lasers (γ_1 and γ_2) are switched on for a short time t_{in} to excite lattice atoms from the ground state to a metastable state via the detuned two-photon (Raman) transition depicted in Figure 4b. Then, during a waiting time Δt in which the lasers are turned off, the atoms tunnel and interact according to equation (1). Finally, the two counter-propagating lasers are turned on for a second time t_{out} , stimulating the decay from the metastable state back to the ground state.

Instead of the perturbation Hamiltonian (3) for the free-space electromagnetic field, we treat the electromagnetic field classically via

$$\hat{V}_{\text{cl}} = g A_{\text{eff}}(t) \hat{\Sigma}^+(\mathbf{\kappa}) + \text{H.c.}, \quad (51)$$

where the atoms in the optical lattice effectively interact with only one mode $\mathbf{\kappa}$, which is given by the momentum difference $\mathbf{\kappa} = \mathbf{k}_1 - \mathbf{k}_2$ of the counter-propagating lasers. Furthermore, $A_{\text{eff}}(t)$ describes the effective classical field of the two counter-propagating lasers, and g denotes an effective coupling constant depending on atomic properties. To simplify the upcoming calculations, we assume it to be real, which leads to

$$\hat{V}_{\text{cl}} = g A_{\text{eff}}(t) [\hat{\Sigma}^+(\mathbf{\kappa}) + \text{H.c.}] = 2g A_{\text{eff}}(t) \hat{\Sigma}^x(\mathbf{\kappa}). \quad (52)$$

Of course, $\hat{\Sigma}^x(\mathbf{\kappa})$ is the generator of a quasispin-rotation about the x -axis. Hence, during the excitation period t_{in} , the quasispin- Z -operator gets rotated by an angle $\alpha = 2g \int_0^{t_{\text{in}}} dt A_{\text{eff}}(t)$, i.e.,

$$\begin{aligned} \hat{\Sigma}_\alpha^z &= \hat{U}_{\text{cl}}^\dagger(\alpha) \hat{\Sigma}^z \hat{U}_{\text{cl}}(\alpha) \\ &= \cos(\alpha) \hat{\Sigma}^z + \sin(\alpha) \hat{\Sigma}^y(\mathbf{\kappa}). \end{aligned} \quad (53)$$

Afterwards, the atoms in the optical lattice can tunnel according to the general lattice Hamiltonian (1). In the weak interactions regime ($U = 0$), the subsequent tunneling (75) over the waiting period Δt can be expressed in the \mathbf{k} -basis via the time-evolution operator

$$\hat{U}_J(\Delta t) = \exp \left\{ i \frac{J\Delta t}{Z} \sum_{\mathbf{k}, s, \lambda} T_{\mathbf{k}} \hat{n}_{\mathbf{k}, s}^\lambda \right\}. \quad (54)$$

Applying the tunneling dynamics to the rotated quasispin- Z -operator, which already contains the excitation process (53), yields

$$\begin{aligned} \hat{\Sigma}_{\alpha, \Delta t}^z &= \hat{U}_J^\dagger(\Delta t) \hat{\Sigma}_\alpha^z \hat{U}_J(\Delta t) \\ &= \cos(\alpha) \hat{\Sigma}^z + \sin(\alpha) \hat{\Sigma}_J^y(\mathbf{\kappa}), \end{aligned} \quad (55)$$

where $\hat{U}_J^\dagger(\Delta t) \hat{\Sigma}^z \hat{U}_J(\Delta t)$ is unchanged (only number operators are involved), while $\hat{\Sigma}_J^y(\mathbf{\kappa})$ picks up mode-specific phases (18) similar to the interaction picture considerations above (19),

$$\begin{aligned} \hat{\Sigma}_J^y(\mathbf{\kappa}) &:= \hat{U}_J^\dagger(\Delta t) \hat{\Sigma}^y(\mathbf{\kappa}) \hat{U}_J(\Delta t) \\ &= \frac{1}{2i} \left(\sum_{\mathbf{p}, s} \hat{a}_{\mathbf{p}, s}^{\text{ex} \dagger} \hat{a}_{\mathbf{p}-\mathbf{\kappa}, s}^{\text{gr}} \exp\{i\phi_{\mathbf{p}}^{\mathbf{\kappa}}(\Delta t)\} - \text{H.c.} \right). \end{aligned} \quad (56)$$

Then, in the third and final step, the counter-propagating lasers are switched on for a second time period t_{out} in order to reverse the rotation α . Hence, we apply the appropriate time-evolution $\hat{U}_{\text{cl}}(\beta)$ with $\beta = 2g \int_0^{t_{\text{out}}} dt A_{\text{eff}}(t)$ to equation (55) to complete the sequence. After some lengthy

but straightforward (commutator) calculations we arrive at:

$$\begin{aligned}\hat{\Sigma}_{\alpha,\Delta t,\beta}^z &= \hat{U}_{\text{cl}}^\dagger(\beta) \hat{\Sigma}_{\alpha,\Delta t}^z \hat{U}_{\text{cl}}(\beta) \\ &= \cos(\alpha) \cos(\beta) \hat{\Sigma}^z + \cos(\alpha) \sin(\beta) \hat{\Sigma}^y(\boldsymbol{\kappa}) \\ &\quad - \sin(\alpha) \sin(\beta) \hat{\Sigma}_C^z(\boldsymbol{\kappa}) + \sin(\alpha) \hat{\Sigma}_C^y(\boldsymbol{\kappa}) \\ &\quad + \sin(\alpha) [\cos(\beta) - 1] \hat{\Sigma}_C^y(\boldsymbol{\kappa}),\end{aligned}\quad (57)$$

where we defined

$$\begin{aligned}\hat{\Sigma}_C^z(\boldsymbol{\kappa}) &:= \frac{1}{2} \sum_{\mathbf{p},s} (\hat{n}_{\mathbf{p},s}^{\text{ex}} - \hat{n}_{\mathbf{p}-\boldsymbol{\kappa},s}^{\text{gr}}) \cos\{\phi_{\mathbf{p}}^{\boldsymbol{\kappa}}(\Delta t)\}, \quad (58) \\ \hat{\Sigma}_C^y(\boldsymbol{\kappa}) &:= \frac{1}{2i} \sum_{\mathbf{p},s} (\hat{a}_{\mathbf{p},s}^{\text{ex}\dagger} \hat{a}_{\mathbf{p}-\boldsymbol{\kappa},s}^{\text{gr}} - \text{H.c.}) \cos\{\phi_{\mathbf{p}}^{\boldsymbol{\kappa}}(\Delta t)\}.\end{aligned}\quad (59)$$

Now, the full sequence is modeled in equation (57). Hence, we can evaluate the expectation value $\langle \Psi | \hat{\Sigma}_{\alpha,\Delta t,\beta}^z | \Psi \rangle$ – which is just the (shifted by $N/2$) number of atoms still excited after the completed sequence – for an arbitrary initial state $|\Psi\rangle$. As before, we only consider initial states $|\Psi\rangle$ which do not contain any excitations. Thus, all $\hat{\Sigma}^y$ -related expectation values vanish, $\langle \Psi | \hat{\Sigma}^z | \Psi \rangle = -N/2$ and

$$\langle \Psi | \hat{\Sigma}_C^z(\boldsymbol{\kappa}) | \Psi \rangle = -\frac{1}{2} \sum_{\mathbf{p},s} n_s(\mathbf{p} - \boldsymbol{\kappa}) \cos\{\phi_{\mathbf{p}}^{\boldsymbol{\kappa}}(\Delta t)\}, \quad (60)$$

where $n_s(\mathbf{p}) = \langle \Psi | \hat{n}_{\mathbf{p},s}^{\text{gr}} | \Psi \rangle$. In summary, we arrive at

$$\begin{aligned}\langle \hat{\Sigma}_{\alpha,\Delta t,\beta}^z \rangle &= -\frac{N}{2} \cos(\alpha) \cos(\beta) + \frac{1}{2} \sin(\alpha) \sin(\beta) \\ &\quad \times \sum_{\mathbf{p},s} n_s(\mathbf{p} - \boldsymbol{\kappa}) \cos\{\phi_{\mathbf{p}}^{\boldsymbol{\kappa}}(\Delta t)\}.\end{aligned}\quad (61)$$

To point out the differences and similarities as compared to the single-photon approach, let us assume very short laser periods $\alpha \ll 1$, $\beta = -\alpha$ (where the sign of $A_{\text{eff}}(t)$ is reversed for the second time period t_{out}) and second order approximation in α . Then, according to (53), $\bar{n} = \langle \hat{\Sigma}^z \rangle + N/2 \approx N\alpha^2/4$ atoms are excited in the first step. If, for example, \bar{n} is smaller than unity, the resulting coherent state is well approximated by a coherent superposition of the ground state $|\text{ground}\rangle$ with $\hat{\Sigma}^-(\boldsymbol{\kappa})|\text{ground}\rangle = 0$ and the first excited Dicke state $\hat{\Sigma}^+(\boldsymbol{\kappa})|\text{ground}\rangle$, which would be the stand-alone result of a single-photon excitation. In the same approximation, the number of atoms still in the metastable state after the full sequence is then given by:

$$\begin{aligned}\langle \hat{n}_{\text{meta}} \rangle &= \langle \hat{\Sigma}_{\alpha,\Delta t,\beta}^z \rangle + \frac{N}{2} \\ &= 2\bar{n} \left(1 - \frac{1}{N} \sum_{\mathbf{p},s} n_s(\mathbf{p} - \boldsymbol{\kappa}) \cos\{\phi_{\mathbf{p}}^{\boldsymbol{\kappa}}(\Delta t)\} \right),\end{aligned}\quad (62)$$

according to equation (61). Inserting, for example, the bosonic partial condensation state with N_1 atoms condensed at $\mathbf{k} = 0$ and N_2 atoms equally distributed over

all \mathbf{k} -modes, which led to the emission probability (30), we find

$$\langle \hat{n}_{\text{meta}} \rangle = 2\bar{n} \left(1 - \frac{N_1}{N} \cos\{\varphi(\Delta t)\} - \frac{N_2}{N} \mathcal{J}(\Delta t) \right), \quad (63)$$

where we considered that the phase-sum over cosine equals the phase-sum over the exponential function (87) in Appendix E, as the imaginary part is zero anyway. Comparing this result to the result of the single-photon approach, we see that we can infer the number N_1 of condensed atoms in both cases – either via the emission characteristics in the single-photon approach (30), or by measuring the number of atoms which are still in the metastable state after the full sequence (63). Going into detail, the term $N_2 \mathcal{J}(\Delta t)$ represents the deterioration of the spatial phase coherence, as in the single-photon approach above. As a consequence, the deexcitation process via the two counter-propagating lasers is hindered, as the altered spatial phases do not fit to the combined laser wave vector $\boldsymbol{\kappa} = \mathbf{k}_1 - \mathbf{k}_2$ anymore. In the quasispin picture, the rotation α about the x -axis (53) would be perfectly rotated back via the second rotation about $\beta = -\alpha$, leading to $\langle \hat{n}_{\text{meta}} \rangle = 0$, if there would be no hopping in between ($J = 0$). For nonzero tunneling $J > 0$, however, the back-rotation is not perfect, which leads to a finite probability for excited atoms remaining in the final state (63). Interestingly, the phase $\varphi(\Delta t)$ occurs in a cosine here, as compared to an exponential phase factor in equation (30). However, this discrepancy is a direct consequence of the classical approach, where we do not create an exact Dicke state but rather a coherent superposition of excited states with different energies. In the quasispin picture, the cosine-term can be understood as a kind of Larmor precession of the quasispin vector about the z -axis during the waiting time Δt .

In conclusion, similar results as in the single-photon approach can be obtained using classical laser fields, which may be more feasible experimentally.

10 Conclusions

In summary, we employed Dicke superradiance, i.e., the collective and coherent absorption and emission of photons, to probe the quantum state, or properties of a quantum phase transition, of an ensemble of ultracold atoms in an optical lattice. In a detailed analysis, we studied both single-photon superradiance (3) as well as superradiance in the context of classical laser fields (51), while the lattice dynamics was modeled via a general lattice Hamiltonian (1), covering both the Bose-Hubbard model and the Fermi-Hubbard model as special cases.

We found that the (single-photon) superradiant emission characteristics are significantly altered due to the lattice dynamics in a variety of scenarios, which can be utilized to obtain information about (the evolution of) the quantum state of the atoms. Considering a bosonic optical lattice in the weak interactions regime ($J \gg U$), (partially) excited states, such as e.g. thermal states, can

be distinguished from condensed states. It may even be possible to infer the number of condensed atoms (30), or the temperature (see Fig 2), respectively. In a fermionic optical lattice, our probe can distinguish the metallic ground state (reduction in superradiance) from the Mott-Néel ground state (no reduction), i.e., detect the current parameter regime ($J \gg U$ or $U \gg J$).

Regarding quantum phase transitions, it is possible to discriminate between an adiabatic transition (no reduction) and a sudden quench transition (reduction in superradiance) from the Mott insulator state to the superfluid phase in a bosonic lattice. Unfortunately, such a distinction can not be made in case of a fermionic lattice, as the superradiance peak decays similarly after either transition (see Fig. 3). Finally, we discussed several options for an experimental realization of the single-photon probing scheme (see Fig. 1), as well as a modified probing sequence employing classical laser fields.

We would like to stress again that our method is complementary to other techniques (e.g., Bragg-scattering), as information about the temporal evolution of the coherence properties of the atoms is encoded in the emission characteristics, and thus can be measured nondestructively. Hence, also non-equilibrium spectral information can be obtained, analogous to pump-probe spectroscopy in solid-state physics. As another topic of recent interest, note that we may distinguish even and odd-frequency correlators [64], as access to double-time Green functions [65] is obtained via the different time coordinates included in the correlator (11). Further research could e.g. focus on whether superconductivity also shows signatures in the correlator (11).

The authors would like to thank Konstantin Krutitsky and Friedemann Queisser for valuable discussions. This work was supported by the DFG (SFB-TR12).

A Correlators \mathcal{C} of the operatorial function \mathcal{D}

To calculate the operatorial function (11) for the case of a separable state with small correlations between lattice sites, it is necessary to go through all possible cases for the correlator (13)

$$\begin{aligned} \mathcal{C}_{s_1 s_2 s_3 s_4}^{\mu\nu\rho\eta}(t, t') = & (\otimes_{\xi} \langle \Psi_{\xi} |) \hat{a}_{\eta s_4}^{\text{gr}\dagger}(t) \hat{a}_{\eta s_4}^{\text{ex}}(t) \hat{a}_{\rho s_3}^{\text{ex}\dagger}(t') \hat{a}_{\rho s_3}^{\text{gr}}(t') \\ & \times \hat{a}_{\mu s_1}^{\text{gr}\dagger}(t') \hat{a}_{\mu s_1}^{\text{ex}}(t') \hat{a}_{\nu s_2}^{\text{ex}\dagger}(t) \hat{a}_{\nu s_2}^{\text{gr}}(t) (\otimes_{\chi} | \Psi_{\chi} \rangle). \end{aligned} \quad (64)$$

First of all, if there is one index η , ρ , μ or ν which does not match any of the other three, the expectation value is zero because then there is always (e.g.) a $\hat{a}_{\eta s_4}^{\text{ex}}$ -annihilation operator working on a single-site state, which, by assumption, contains no $\hat{a}_{\eta s_4}^{\text{ex}\dagger}$ -excitations, i.e.,

$$\langle \Psi_{\eta} | \hat{a}_{\eta s_4}^{\text{gr}\dagger}(t) \hat{a}_{\eta s_4}^{\text{ex}}(t) | \Psi_{\eta} \rangle = 0. \quad (65)$$

Thus we are left with four possibly nonzero cases – three with two pairs and one where all indices are the same.

While the case $\mathcal{C}^{\mu\mu\eta\eta}$ was already discussed in Section 4, the cases $\mathcal{C}^{\rho\eta\rho\eta}$ and $\mathcal{C}^{\eta\rho\rho\eta}$ are zero because, e.g.,

$$\begin{aligned} \mathcal{C}_{s_1 s_2 s_3 s_4}^{\eta\rho\rho\eta}(t, t') = & \langle \Psi_{\eta} | \langle \Psi_{\rho} | \hat{a}_{\eta s_4}^{\text{gr}\dagger}(t) \hat{a}_{\eta s_4}^{\text{ex}}(t) \hat{a}_{\rho s_3}^{\text{ex}\dagger}(t') \hat{a}_{\rho s_3}^{\text{gr}}(t') \\ & \times \hat{a}_{\eta s_1}^{\text{gr}\dagger}(t') \hat{a}_{\eta s_1}^{\text{ex}}(t') | \Psi_{\eta} \rangle \hat{a}_{\rho s_2}^{\text{ex}\dagger}(t) \hat{a}_{\rho s_2}^{\text{gr}}(t) | \Psi_{\rho} \rangle = 0. \end{aligned} \quad (66)$$

When all four indices are the same, $\mathcal{C}^{\eta\eta\eta\eta}$, the result is (in general) nonzero. It can be neglected, however, as for this case the operatorial part (11) at most scales with N – as opposed to N^2 in the case of $\mathcal{C}^{\mu\mu\eta\eta}$. Hence, to leading order in N , the operatorial part for separable states is given by equation (15).

B Emission probability density for a single atom

Throughout this paper, we often compare the collective emission probability density from the atoms in the optical lattice to the emission probability in case of a single atom. The special case that there is only a single atom (without spin quantum number, i.e., index s omitted) $|\Psi\rangle = |1\rangle^{\text{gr}} \otimes |0\rangle^{\text{ex}}$ absorbing and re-emitting the photon corresponds to an operatorial part in equation (8) of just

$$\begin{aligned} \hat{\Sigma}^-(\kappa_{\text{out}}, t_2) \hat{\Sigma}^+(\kappa_{\text{in}}, t_1) = & \hat{a}^{\text{gr}\dagger}(t_2) \hat{a}^{\text{ex}}(t_2) \hat{a}^{\text{ex}\dagger}(t_1) \hat{a}^{\text{gr}}(t_1) \exp\{-i(\kappa_{\text{out}} - \kappa_{\text{in}}) \mathbf{r}\} = \\ & \hat{a}^{\text{gr}\dagger} \hat{a}^{\text{ex}} \hat{a}^{\text{ex}\dagger} \hat{a}^{\text{gr}} e^{i\omega(t_1 - t_2)} \exp\{-i(\kappa_{\text{out}} - \kappa_{\text{in}}) \mathbf{r}\}, \end{aligned} \quad (67)$$

because $\hat{H}_{\text{lat}} = 0$ and thus, $\hat{H} - \hat{V}$ becomes trivial. Accordingly, P reduces to P_{single} (assuming resonance $\omega_{\text{in}} = \omega$),

$$P_{\text{single}} = \mathcal{I} \left[e^{i(\omega_{\text{out}} - \omega)t_2} \right]. \quad (68)$$

Not surprisingly, the emission in case of a single atom is not directed. Note that we assume that the emission probability of a single atom is independent of a potential spin quantum number s . We would expect the same emission probability density (68) in the case of a single fermionic atom, irregardless of its spin state.

C General lattice Hamiltonian in \mathbf{k} -basis

In the limiting case of weak interactions ($J \gg U$), we approximate $U = 0$, i.e., the on-site repulsion term vanishes from the general lattice Hamiltonian (1), and only the tunneling term remains,

$$\hat{H}_J = -\frac{J}{Z} \sum_{\mu\nu, s, \lambda} T_{\mu\nu} \hat{a}_{\mu s}^{\lambda\dagger} \hat{a}_{\nu s}^{\lambda}. \quad (69)$$

The Hamiltonian can be diagonalized using a Fourier transform to the \mathbf{k} -basis, where the summation runs over all lattice vectors $\mathbf{k} = \{n, m\} \frac{2\pi}{L}$, with $n, m \in \{-L/2 + 1, \dots, L/2\}$,

where L is the number of lattice sites per dimension ($L^2 = N$),

$$\hat{a}_{\mu s}^{\lambda \dagger} = \frac{1}{\sqrt{N}} \sum_{\mathbf{k}} \hat{a}_{\mathbf{k},s}^{\lambda \dagger} \exp \{-i\mathbf{k} \cdot \mathbf{r}_{\mu}\}. \quad (70)$$

Applying these on the Hamiltonian (69), we get at first

$$\hat{H}_J = -\frac{J}{NZ} \sum_{\mu\nu \mathbf{k}\mathbf{p},s,\lambda} T_{\mu\nu} \hat{a}_{\mathbf{k},s}^{\lambda \dagger} \hat{a}_{\mathbf{p},s}^{\lambda} \times \exp \{-i\mathbf{k} \cdot \mathbf{r}_{\mu}\} \exp \{i\mathbf{p} \cdot \mathbf{r}_{\nu}\}. \quad (71)$$

However, for a 2D-lattice, the summation over the four nearest neighbors yields

$$\sum_{\nu} T_{\mu\nu} \exp \{i\mathbf{p} \cdot \mathbf{r}_{\nu}\} = T_{\mathbf{p}} \exp \{i\mathbf{p} \cdot \mathbf{r}_{\mu}\}, \quad (72)$$

with $T_{\mathbf{p}}$ the Fourier transform of the adjacency matrix,

$$T_{\mathbf{p}} = 2 [\cos(p_x \ell) + \cos(p_y \ell)]. \quad (73)$$

In addition, as \mathbf{k} and \mathbf{p} are both lattice vectors, the μ -summation is non-vanishing only for $\mathbf{k} = \mathbf{p}$, i.e.,

$$\sum_{\mu} \exp \{i(\mathbf{p} - \mathbf{k}) \cdot \mathbf{r}_{\mu}\} = N \delta_{\mathbf{k}\mathbf{p}}. \quad (74)$$

Employing the relations (72) and (74), we arrive at the diagonalized tunneling Hamiltonian in \mathbf{k} -basis

$$\hat{H}_J = -\frac{J}{Z} \sum_{\mathbf{k},s,\lambda} T_{\mathbf{k}} \hat{a}_{\mathbf{k},s}^{\lambda \dagger} \hat{a}_{\mathbf{k},s}^{\lambda} = -\frac{J}{Z} \sum_{\mathbf{k},s,\lambda} T_{\mathbf{k}} \hat{n}_{\mathbf{k},s}^{\lambda}. \quad (75)$$

D Four-point correlators in the bosonic and fermionic case

D.1 Correlator in the bosonic case

The most explanatory way to calculate the bosonic four-point correlator in equation (21),

$$E_n^B = \langle \Psi | \hat{a}_{\mathbf{q}-\kappa_{\text{in}}}^{\text{gr} \dagger} \hat{a}_{\mathbf{q}-\kappa_{\text{out}}}^{\text{gr}} \hat{a}_{\mathbf{k}-\kappa_{\text{out}}}^{\text{gr} \dagger} \hat{a}_{\mathbf{k}-\kappa_{\text{in}}}^{\text{gr}} | \Psi \rangle, \quad (76)$$

is by going through the cases which can yield a nonzero result. Obviously, the two creation operators have to compensate for the two annihilation operators, such that in the end, the basis-state $|\Psi\rangle$ is unchanged. This is the case when either $\mathbf{k} - \kappa_{\text{in}} = \mathbf{k} - \kappa_{\text{out}}$ and $\mathbf{q} - \kappa_{\text{out}} = \mathbf{q} - \kappa_{\text{in}}$, or $\mathbf{k} - \kappa_{\text{in}} = \mathbf{q} - \kappa_{\text{in}}$ and $\mathbf{k} - \kappa_{\text{out}} = \mathbf{q} - \kappa_{\text{out}}$, i.e.,

$$\begin{aligned} E_n^B &= \delta_{\mathbf{k}-\kappa_{\text{in}}, \mathbf{k}-\kappa_{\text{out}}} \delta_{\mathbf{q}-\kappa_{\text{out}}, \mathbf{q}-\kappa_{\text{in}}} \langle \Psi | \hat{n}_{\mathbf{q}-\kappa_{\text{out}}}^{\text{gr}} \hat{n}_{\mathbf{k}-\kappa_{\text{in}}}^{\text{gr}} | \Psi \rangle \\ &+ \delta_{\mathbf{k}-\kappa_{\text{in}}, \mathbf{q}-\kappa_{\text{in}}} \delta_{\mathbf{k}-\kappa_{\text{out}}, \mathbf{q}-\kappa_{\text{out}}} \langle \Psi | \hat{a}_{\mathbf{k}-\kappa_{\text{in}}}^{\text{gr} \dagger} \hat{a}_{\mathbf{q}-\kappa_{\text{out}}}^{\text{gr}} \hat{a}_{\mathbf{q}-\kappa_{\text{out}}}^{\text{gr} \dagger} \hat{a}_{\mathbf{k}-\kappa_{\text{in}}}^{\text{gr}} | \Psi \rangle \\ &\times (1 - \delta_{\mathbf{k}-\kappa_{\text{in}}, \mathbf{q}-\kappa_{\text{out}}}), \end{aligned} \quad (77)$$

where the case that all four operators work on the same \mathbf{k} -vector was excluded in the last line, as it is already included in the first term. Further simplifications yield

$$\begin{aligned} E_n^B &= \delta_{\kappa_{\text{in}} \kappa_{\text{out}}} \langle \Psi | \hat{n}_{\mathbf{q}-\kappa_{\text{out}}}^{\text{gr}} \hat{n}_{\mathbf{k}-\kappa_{\text{in}}}^{\text{gr}} | \Psi \rangle \\ &+ \delta_{\mathbf{k}\mathbf{q}} \langle \Psi | (\hat{n}_{\mathbf{q}-\kappa_{\text{out}}}^{\text{gr}} + 1) \hat{n}_{\mathbf{k}-\kappa_{\text{in}}}^{\text{gr}} | \Psi \rangle (1 - \delta_{\kappa_{\text{in}} \kappa_{\text{out}}}). \end{aligned} \quad (78)$$

And with $\hat{n}_{\mathbf{k}}^{\text{gr}} |\Psi\rangle = n(\mathbf{k}) |\Psi\rangle$, where $|\Psi\rangle$ is of course normalized, we arrive at the result

$$\begin{aligned} E_n^B &= n(\mathbf{k} - \kappa_{\text{in}}) n(\mathbf{q} - \kappa_{\text{out}}) (\delta_{\kappa_{\text{in}} \kappa_{\text{out}}} + \delta_{\mathbf{k}\mathbf{q}}) \\ &+ n(\mathbf{k} - \kappa_{\text{in}}) \delta_{\mathbf{k}\mathbf{q}} \\ &- n(\mathbf{k} - \kappa_{\text{in}}) [n(\mathbf{q} - \kappa_{\text{out}}) + 1] \delta_{\mathbf{k}\mathbf{q}} \delta_{\kappa_{\text{in}} \kappa_{\text{out}}}. \end{aligned} \quad (79)$$

D.2 Correlator in the fermionic case

The fermionic correlator from equation (21),

$$E_n^F = \langle \Psi | \hat{a}_{\mathbf{q}-\kappa_{\text{in}},s_2}^{\text{gr} \dagger} \hat{a}_{\mathbf{q}-\kappa_{\text{out}},s_2}^{\text{gr}} \hat{a}_{\mathbf{k}-\kappa_{\text{out}},s_1}^{\text{gr} \dagger} \hat{a}_{\mathbf{k}-\kappa_{\text{in}},s_1}^{\text{gr}} | \Psi \rangle, \quad (80)$$

can be calculated analogous to the bosonic case, although some differences arise. Again, a nonzero result is obtained when $\mathbf{k} - \kappa_{\text{in}} = \mathbf{k} - \kappa_{\text{out}}$, $\mathbf{q} - \kappa_{\text{out}} = \mathbf{q} - \kappa_{\text{in}}$ and spins s_1, s_2 arbitrary. The other possible combination is when $\mathbf{k} - \kappa_{\text{in}} = \mathbf{q} - \kappa_{\text{in}}$, $\mathbf{k} - \kappa_{\text{out}} = \mathbf{q} - \kappa_{\text{out}}$ and the spins $s_1 = s_2$ are equal,

$$\begin{aligned} E_n^F &= \delta_{\mathbf{k}-\kappa_{\text{in}}, \mathbf{k}-\kappa_{\text{out}}} \delta_{\mathbf{q}-\kappa_{\text{out}}, \mathbf{q}-\kappa_{\text{in}}} \langle \Psi | \hat{n}_{\mathbf{q}-\kappa_{\text{out}},s_2}^{\text{gr}} \hat{n}_{\mathbf{k}-\kappa_{\text{in}},s_1}^{\text{gr}} | \Psi \rangle \\ &+ \delta_{\mathbf{k}-\kappa_{\text{in}}, \mathbf{q}-\kappa_{\text{in}}} \delta_{\mathbf{k}-\kappa_{\text{out}}, \mathbf{q}-\kappa_{\text{out}}} \delta_{s_1 s_2} (1 - \delta_{\mathbf{k}-\kappa_{\text{in}}, \mathbf{q}-\kappa_{\text{out}}}) \\ &\times \langle \Psi | \hat{a}_{\mathbf{k}-\kappa_{\text{in}},s_1}^{\text{gr} \dagger} \hat{a}_{\mathbf{q}-\kappa_{\text{out}},s_1}^{\text{gr}} \hat{a}_{\mathbf{q}-\kappa_{\text{out}},s_1}^{\text{gr} \dagger} \hat{a}_{\mathbf{k}-\kappa_{\text{in}},s_1}^{\text{gr}} | \Psi \rangle, \end{aligned} \quad (81)$$

where, again, the case of all four \mathbf{k} -vectors equal was excluded from the second term to prevent it being included twice. After simplifying the Kronecker deltas and applying anti-commutation relations to the second term, we arrive at:

$$\begin{aligned} E_n^F &= \delta_{\kappa_{\text{in}} \kappa_{\text{out}}} \langle \Psi | \hat{n}_{\mathbf{q}-\kappa_{\text{out}},s_2}^{\text{gr}} \hat{n}_{\mathbf{k}-\kappa_{\text{in}},s_1}^{\text{gr}} | \Psi \rangle \\ &+ \delta_{\mathbf{k}\mathbf{q}} \delta_{s_1 s_2} (1 - \delta_{\kappa_{\text{in}} \kappa_{\text{out}}}) \\ &\times \langle \Psi | (1 - \hat{n}_{\mathbf{q}-\kappa_{\text{out}},s_1}^{\text{gr}}) \hat{n}_{\mathbf{k}-\kappa_{\text{in}},s_1}^{\text{gr}} | \Psi \rangle. \end{aligned} \quad (82)$$

This expression resembles the result of the bosonic case (78), but is not quite the same. The difference becomes even more apparent when we consider that we can omit the $\delta_{\kappa_{\text{in}} \kappa_{\text{out}}}$ in the second line, as in the fermionic case $(\hat{n}_{\mathbf{k}-\kappa_{\text{in}},s_1}^{\text{gr}})^2 = \hat{n}_{\mathbf{k}-\kappa_{\text{in}},s_1}^{\text{gr}}$, i.e., the expectation value already becomes zero for $\kappa_{\text{in}} = \kappa_{\text{out}}$ (and $\mathbf{k} = \mathbf{q}$),

$$\begin{aligned} E_n^F &= \delta_{\kappa_{\text{in}} \kappa_{\text{out}}} \langle \Psi | \hat{n}_{\mathbf{q}-\kappa_{\text{out}},s_2}^{\text{gr}} \hat{n}_{\mathbf{k}-\kappa_{\text{in}},s_1}^{\text{gr}} | \Psi \rangle \\ &+ \delta_{\mathbf{k}\mathbf{q}} \delta_{s_1 s_2} \langle \Psi | (1 - \hat{n}_{\mathbf{q}-\kappa_{\text{out}},s_1}^{\text{gr}}) \hat{n}_{\mathbf{k}-\kappa_{\text{in}},s_1}^{\text{gr}} | \Psi \rangle. \end{aligned} \quad (83)$$

Expressed via the occupation numbers $\hat{n}_{\mathbf{k},s}^{\text{gr}} |\Psi\rangle = n_s(\mathbf{k}) |\Psi\rangle$, we come to the final result

$$\begin{aligned} E_n^F &= n_{s_1}(\mathbf{k} - \kappa_{\text{in}}) n_{s_2}(\mathbf{q} - \kappa_{\text{out}}) (\delta_{\kappa_{\text{in}} \kappa_{\text{out}}} - \delta_{\mathbf{k}\mathbf{q}} \delta_{s_1 s_2}) \\ &+ n_{s_1}(\mathbf{k} - \kappa_{\text{in}}) \delta_{\mathbf{k}\mathbf{q}} \delta_{s_1 s_2}. \end{aligned} \quad (84)$$

Emission probability of the partial condensation state

In this section, we derive the emission probability density of the partial condensation state (30), which contains a certain number N_1 of bosons in the ground state at $\mathbf{k} = 0$ while the other N_2 bosons should be equally distributed between all \mathbf{k} -modes⁸. Inserting the corresponding number distribution $n^{\text{dt}}(\mathbf{k}) = N_1\delta_{\mathbf{k}0} + N_2/N$ into the expression for the bosonic four-point correlator (22) yields a lengthy result,

$$\begin{aligned} E_{n^{\text{dt}}}^{\text{B}} = & N_1^2 \delta_{\mathbf{kq}\kappa_{\text{in}}\kappa_{\text{out}}} \\ & + \frac{N_1 N_2}{N} (\delta_{\mathbf{k}\kappa_{\text{in}}\kappa_{\text{out}}} + \delta_{\mathbf{q}\kappa_{\text{in}}\kappa_{\text{out}}} \\ & \quad + \delta_{\mathbf{kq}\kappa_{\text{in}}} + \delta_{\mathbf{kq}\kappa_{\text{out}}} - 2\delta_{\mathbf{kq}\kappa_{\text{in}}\kappa_{\text{out}}}) \\ & + N_1 (\delta_{\mathbf{kq}\kappa_{\text{in}}} - \delta_{\mathbf{kq}\kappa_{\text{in}}\kappa_{\text{out}}}) \\ & + \frac{N_2^2}{N^2} (\delta_{\kappa_{\text{in}}\kappa_{\text{out}}} + \delta_{\mathbf{kq}} - \delta_{\mathbf{kq}}\delta_{\kappa_{\text{in}}\kappa_{\text{out}}}) \\ & + \frac{N_2}{N} (\delta_{\mathbf{kq}} - \delta_{\mathbf{kq}}\delta_{\kappa_{\text{in}}\kappa_{\text{out}}}) . \end{aligned} \quad (85)$$

However, assuming that N_1 , N_2 and N are of the same order $\mathcal{O}(N) \gg 1$, we can omit all terms of order $\mathcal{O}(N)$ or lower from $E_{n^{\text{dt}}}^{\text{B}}$, i.e., keep only terms of quadratic order $\mathcal{O}(N^2)$. Note that the summation over the indices \mathbf{k} and \mathbf{q} in equation (21) in general also yields a factor of order $\mathcal{O}(N)$ each, and thus it is important whether these indices are fixed or free in the respective term. For example, the term $N_1 N_2 / N \delta_{\mathbf{kq}\kappa_{\text{in}}}$ in the third line in equation (85) only scales with $\mathcal{O}(N)$, due to the prefactor, as both indices \mathbf{k} and \mathbf{q} are fixed. This is in opposition to, e.g., the terms of the second line in equation (85). After omitting all terms of order $\mathcal{O}(N)$ or lower, which correspond to incoherent emission processes, the remaining terms,

$$\begin{aligned} \tilde{E}_{n^{\text{dt}}}^{\text{B}} = & \left(N_1^2 \delta_{\mathbf{kq}\kappa_{\text{out}}} + \frac{N_1 N_2}{N} (\delta_{\mathbf{k}\kappa_{\text{out}}} + \delta_{\mathbf{q}\kappa_{\text{out}}}) + \frac{N_2^2}{N^2} \right) \\ & \times \delta_{\kappa_{\text{in}}\kappa_{\text{out}}} , \end{aligned} \quad (86)$$

carry the factor $\delta_{\kappa_{\text{in}}\kappa_{\text{out}}}$, that is, they represent superradiant emission in the same direction in which the absorbed photon was incoming, $\kappa_{\text{out}} = \kappa_{\text{in}}$. When we insert (86) into the operatorial part \mathcal{E} in equation (21), we can thus combine the phases in the exponentials. After we have introduced $\kappa = \kappa_{\text{in}} = \kappa_{\text{out}}$, $\varphi(\Delta t) = -\phi_{\kappa}^{\kappa}(\Delta t)$ and the

⁸ Strictly speaking, the presented partial condensation state is neither a pure state diagonal in the \mathbf{k} -basis nor a Gaussian state, when $N_{1/2}$ are chosen such that N_2/N is not an integer. However, there are two possible ways out, such that the partial condensation state can be expressed as a pure state. One could either consider a lattice with more atoms N_{ψ} than lattice sites N to make sure that N_2/N is integer, or one can think of distributing the N_2 bosons only almost equally (e.g., checkerboard pattern), such that the number of bosons in a certain \mathbf{k} -mode is always integer.

phase-sum \mathcal{J} as abbreviations,

$$\mathcal{J}(\Delta t) = \frac{1}{N} \sum_{\mathbf{p}} \exp \{ iJ/Z(T_{\mathbf{p}} - T_{\mathbf{p}-\kappa})\Delta t \} \leq 1 , \quad (87)$$

the operatorial part reads

$$\begin{aligned} \mathcal{E}(t_1, t_2, t_3, t_4) = & \left[N_1^2 e^{i\varphi(t_3-t_4)} e^{i\varphi(t_2-t_1)} \right. \\ & + N_1 N_2 \left(\mathcal{J}(t_3 - t_4) e^{i\varphi(t_2-t_1)} + \mathcal{J}(t_2 - t_1) e^{i\varphi(t_3-t_4)} \right) \\ & \left. + N_2^2 \mathcal{J}(t_3 - t_4) \mathcal{J}(t_2 - t_1) \right] \delta_{\kappa_{\text{in}}\kappa_{\text{out}}} . \end{aligned} \quad (88)$$

Finally, we can evaluate the emission probability density (20). It can be written as an absolute square depending on the waiting time $\Delta t = t_2 - t_1$ times the single-atom emission probability density P_{single} (when we again regard Δt as constant over the integration periods, see above),

$$P = \left| N_1 e^{i\varphi(\Delta t)} + N_2 \mathcal{J}(\Delta t) \right|^2 \delta_{\kappa_{\text{in}}\kappa_{\text{out}}} P_{\text{single}} . \quad (89)$$

F Approximation of the phase-sum $\mathcal{J}(\Delta t)$ via Bessel functions

The phase-sum (87),

$$\mathcal{J}(\Delta t) = \frac{1}{N} \sum_{\mathbf{p}} \exp \{ iJ/Z(T_{\mathbf{p}} - T_{\mathbf{p}-\kappa})\Delta t \} , \quad (90)$$

can be approximated when the photon wave number κ is small compared to the inverse of the lattice constant ℓ . In this case, we can Taylor-approximate the argument of the exponential,

$$\begin{aligned} (T_{\mathbf{p}} - T_{\mathbf{p}-\kappa}) & \approx \kappa \cdot \nabla_{\mathbf{p}} T_{\mathbf{p}} \big|_{\mathbf{p}} \\ & = -2\ell [\kappa_x \sin(p_x \ell) + \kappa_y \sin(p_y \ell)] . \end{aligned} \quad (91)$$

And split the phase-sum \mathcal{J} in equation (90) into a x - and a y -part,

$$\mathcal{J}(\Delta t) = \mathcal{J}^x(\Delta t) \times \mathcal{J}^y(\Delta t) , \quad (92)$$

with the one-dimensional sums over the L values of p_x or p_y (where L is the number of lattice sites in one dimension, i.e., $L^2 = N$),

$$\mathcal{J}^{x/y}(\Delta t) := \frac{1}{L} \sum_{p_{x/y}} \exp \{ -i2\ell J/Z \kappa_{x/y} \sin(p_{x/y} \ell) \Delta t \} . \quad (93)$$

These one-dimensional sums can now be approximated as (cylindrical) Bessel functions when going to the integral

(justified for $L \gg 1$),

$$\begin{aligned} \mathcal{J}^{x/y}(\Delta t) &= \frac{1}{L} \sum_{n=-L/2+1}^{L/2} \exp \left\{ -i2\ell J/Z \kappa_{x/y} \sin(n2\pi/L) \Delta t \right\} \\ &\approx \frac{1}{L} \int_{-L/2}^{L/2} d\lambda \exp \left\{ -i2\ell J/Z \kappa_{x/y} \sin(\lambda 2\pi/L) \Delta t \right\}, \end{aligned} \quad (94)$$

and substituting by $z = \lambda 2\pi/L$,

$$\begin{aligned} \mathcal{J}^{x/y}(\Delta t) &\approx \frac{1}{2\pi} \int_{-\pi}^{\pi} dz \exp \left\{ -i2\ell J/Z \kappa_{x/y} \sin(z) \Delta t \right\} \\ &= J_0 \left(-2 \frac{J\Delta t}{Z} \kappa_{x/y} \right). \end{aligned} \quad (95)$$

Thus, in summary, the phase-sum (87) can be approximated via

$$\mathcal{J}(\Delta t) \approx J_0 \left(2 \frac{J\Delta t}{Z} \kappa_x \right) J_0 \left(2 \frac{J\Delta t}{Z} \kappa_y \right), \quad (96)$$

where the minus signs were dropped as the Bessel functions J_0 are even.

G Four-point correlators in the Mott state and Mott-Néel state

To calculate the four-point correlator in the Mott state (26) or the Mott-Néel state (35),

$$\begin{aligned} E_{\text{Mo/Né}}^{\text{B/F}} &= \langle \Psi_{\text{Mo/Né}}^{J=0} | \hat{a}_{\mathbf{q}-\kappa_{\text{in}},s_2}^{\text{gr}\dagger} \hat{a}_{\mathbf{q}-\kappa_{\text{out}},s_2}^{\text{gr}} \\ &\quad \times \hat{a}_{\mathbf{k}-\kappa_{\text{out}},s_1}^{\text{gr}\dagger} \hat{a}_{\mathbf{k}-\kappa_{\text{in}},s_1}^{\text{gr}} | \Psi_{\text{Mo/Né}}^{J=0} \rangle, \end{aligned} \quad (97)$$

we transfer the creation and annihilation operators back to the lattice site basis via

$$\hat{a}_{\mathbf{k},s}^{\lambda\dagger} = \frac{1}{\sqrt{N}} \sum_{\mu} \hat{a}_{\mu s}^{\lambda\dagger} \exp \{ i\mathbf{k} \cdot \mathbf{r}_{\mu} \}, \quad (98)$$

leading to the expression

$$\begin{aligned} E_{\text{Mo/Né}}^{\text{B/F}} &= \frac{1}{N^2} \sum_{\mu\nu\rho\eta} e^{i(\mathbf{k}-\kappa_{\text{out}})\mathbf{r}_{\mu}} e^{-i(\mathbf{k}-\kappa_{\text{in}})\mathbf{r}_{\nu}} \\ &\quad \times e^{-i(\mathbf{q}-\kappa_{\text{out}})\mathbf{r}_{\rho}} e^{i(\mathbf{q}-\kappa_{\text{in}})\mathbf{r}_{\eta}} \\ &\quad \times \langle \Psi_{\text{Mo/Né}}^{J=0} | \hat{a}_{\eta s_2}^{\text{gr}\dagger} \hat{a}_{\rho s_2}^{\text{gr}} \hat{a}_{\mu s_1}^{\text{gr}\dagger} \hat{a}_{\nu s_1}^{\text{gr}} | \Psi_{\text{Mo/Né}}^{J=0} \rangle. \end{aligned} \quad (99)$$

As now both the operators and the states are given in the lattice site basis, the expectation value in the last line can be readily calculated. For the case of bosons (i.e., index s omitted) and the Mott insulator state, we get

$$\begin{aligned} \langle \Psi_{\text{Mo}}^{J=0} | \hat{b}_{\eta}^{\text{gr}\dagger} \hat{b}_{\rho}^{\text{gr}} \hat{b}_{\mu}^{\text{gr}\dagger} \hat{b}_{\nu}^{\text{gr}} | \Psi_{\text{Mo}}^{J=0} \rangle &= \\ \delta_{\mu\nu} \delta_{\rho\eta} + 2\delta_{\nu\eta} \delta_{\mu\rho} - 2\delta_{\mu\nu} \delta_{\rho\eta}, \end{aligned} \quad (100)$$

and thus

$$E_{\text{Mo}}^{\text{B}} = \delta_{\kappa_{\text{in}}\kappa_{\text{out}}} + 2\delta_{\mathbf{k}\mathbf{q}} - 2/N. \quad (101)$$

For the case of fermions and the Mott-Néel state, we get

$$\begin{aligned} \langle \Psi_{\text{Né}}^{J=0} | \hat{c}_{\eta s_2}^{\text{gr}\dagger} \hat{c}_{\rho s_2}^{\text{gr}} \hat{c}_{\mu s_1}^{\text{gr}\dagger} \hat{c}_{\nu s_1}^{\text{gr}} | \Psi_{\text{Né}}^{J=0} \rangle &= \delta_{\mu\nu} \delta_{\rho\eta} \delta_{s_1 s_\nu} \delta_{s_2 s_\rho} \\ &\quad + \delta_{\nu\eta} \delta_{\mu\rho} \delta_{s_1 s_2 s_\nu} - \delta_{\nu\eta} \delta_{\mu\rho} \delta_{s_1 s_2 s_\nu s_\mu}, \end{aligned} \quad (102)$$

where the s_ν refer to the spin of the atom at lattice site ν in the Mott-Néel state, and so forth. Inserting in (99), and summing over the spin indices s_1, s_2 , yields

$$\begin{aligned} \sum_{s_1 s_2} E_{\text{Né}}^{\text{F}} &= \delta_{\kappa_{\text{in}}\kappa_{\text{out}}} + \delta_{\mathbf{k}\mathbf{q}} \\ &\quad - \frac{1}{N^2} \sum_{\mu\nu} e^{i(\mathbf{k}-\mathbf{q})\mathbf{r}_{\mu}} e^{-i(\mathbf{k}-\mathbf{q})\mathbf{r}_{\nu}} \delta_{s_\nu s_\mu}. \end{aligned} \quad (103)$$

The third term can be calculated by splitting the sums according to the two sub-lattices \mathcal{A} and \mathcal{B} (see above), which yields two contributions with $(N/2)^2$ summands each, i.e., together they give $N^2 \delta_{\mathbf{k}\mathbf{q}}/2$, and thus,

$$\sum_{s_1 s_2} E_{\text{Né}}^{\text{F}} = \delta_{\kappa_{\text{in}}\kappa_{\text{out}}} + \delta_{\mathbf{k}\mathbf{q}}/2. \quad (104)$$

H Adiabatic transition in a bosonic lattice

In the bosonic case, the excited state (40) reads

$$|\Psi\rangle_{\text{ex}}^{\text{Mo}} \propto \frac{1}{\sqrt{N}} \sum_{\mu} \exp \{ i\kappa_{\text{in}} \cdot \mathbf{r}_{\mu} \} \hat{b}_{\mu}^{\text{ex}\dagger} \prod_{\nu \neq \mu} \hat{b}_{\nu}^{\text{gr}\dagger} |0\rangle, \quad (105)$$

where the $|0\rangle$ -kets refers to the vacuum state of both the lattice bosons and the photon field. Note that after the absorption of the probe photon κ_{in} , the lattice state lives in the subspace where one atom is excited and the other $N-1$ atoms are not, and stays in that subspace during the adiabatic evolution and the following waiting time, i.e., until the probe photon is re-emitted. Moreover, in the separable state regime ($U \gg J$), the state (105) is an approximate eigenstate of the two-species Bose-Hubbard Hamiltonian (24), when κ_{in} is a lattice vector (what we require). We know from the adiabatic theorem that an initial eigenstate such as (105) stays an eigenstate during the adiabatic evolution, and we end up with a corresponding eigenstate of the new ($U=0$) Hamiltonian. For $N \gg 1$, this corresponding eigenstate (with the same prefactor stemming from the absorption) is given by

$$|\Psi\rangle_{\text{ex}}^{\text{sf}} \propto \frac{1}{\sqrt{(N-1)!}} (\hat{b}_{\mathbf{k}=0}^{\text{gr}\dagger})^{N-1} \hat{b}_{\kappa_{\text{in}}}^{\text{ex}\dagger} |0\rangle, \quad (106)$$

i.e., with $N-1$ atoms in the superfluid state at $\mathbf{k}=0$, while the excited atom carries the wave vector κ_{in} of the absorbed photon. The emission probability after the adiabatic transition can be calculated analog to (41). As a shortcut, the state (106) can be understood as exciton

creation applied to the superfluid ground state, i.e., the emission probability can be evaluated via

$$\hat{\Sigma}_J^-(\kappa_{\text{out}}, t_2) \hat{\Sigma}_U^+(\kappa_{\text{in}}, t_1) |\Psi\rangle_{\text{sf}}^{U=0} = e^{i\omega(t_1-t_2)} \times \sum_{\mathbf{k}} \exp\{-i\phi_{\mathbf{k}}^{\text{out}}(t_2)\} \hat{b}_{\mathbf{k}-\kappa_{\text{out}}}^{\text{gr}\dagger} \hat{b}_{\mathbf{k}-\kappa_{\text{in}}}^{\text{gr}} |\Psi\rangle_{\text{sf}}^{U=0}, \quad (107)$$

which leads back to the already known four-point correlator of the superfluid ground state (28). Connecting the parts we obtain in leading order in N

$$P = N^2 \delta_{\kappa_{\text{in}} \kappa_{\text{out}}} \mathcal{I} \left[e^{i(\omega_{\text{out}} - \omega)t_2} e^{i\varphi(t_2)} \right], \quad (108)$$

where, thanks to the properties of the superfluid ground state, the \mathbf{k} -sums are fixed and only a single phase factor $e^{i\varphi(t_2)}$ remains. This phase can be neglected, however, as the tunneling rate J is small compared to the optical energies in the temporal phase. Thus we arrive at the result of usual, full superradiance,

$$P = N^2 \delta_{\kappa_{\text{in}} \kappa_{\text{out}}} P_{\text{single}}. \quad (109)$$

References

1. I. Bloch, *Phys. World* **17**, 25 (2004)
2. M. Raizen, C. Salomon, Q. Niu, *Phys. Today* **50**, 30 (1997)
3. I. Bloch, *Nat. Phys.* **1**, 23 (2005)
4. I. Bloch, J. Dalibard, W. Zwerger, *Rev. Mod. Phys.* **80**, 885 (2008)
5. D. Jaksch, P. Zoller, *Ann. Phys.* **315**, 52 (2005)
6. S. Sachdev, *Quantum Phase Transitions*, 2nd edn. (Cambridge University Press, Cambridge, 2011)
7. M.P.A. Fisher, P.B. Weichman, G. Grinstein, D.S. Fisher, *Phys. Rev. B* **40**, 546 (1989)
8. D. Jaksch, C. Bruder, J.I. Cirac, C.W. Gardiner, P. Zoller, *Phys. Rev. Lett.* **81**, 3108 (1998)
9. K.V. Krutitsky, *Phys. Rep.* **607**, 1 (2016)
10. M. Greiner, O. Mandel, T. Esslinger, T.W. Hansch, I. Bloch, *Nature* **415**, 39 (2002)
11. T. Stöferle, H. Moritz, C. Schori, M. Köhl, T. Esslinger, *Phys. Rev. Lett.* **92**, 130403 (2004)
12. I.B. Spielman, W.D. Phillips, J.V. Porto, *Phys. Rev. Lett.* **98**, 080404 (2007)
13. Y. Kato, Q. Zhou, N. Kawashima, N. Trivedi, *Nat. Phys.* **4**, 617 (2008)
14. G.K. Campbell, J. Mun, M. Boyd, P. Medley, A.E. Leanhardt, L.G. Marcassa, D.E. Pritchard, W. Ketterle, *Science* **313**, 649 (2006)
15. H. Miyake, G.A. Siviloglou, G. Puentes, D.E. Pritchard, W. Ketterle, D.M. Weld, *Phys. Rev. Lett.* **107**, 175302 (2011)
16. J. Hubbard, *Proc. Roy. Soc. A* **276**, 238 (1963)
17. N.F. Mott, *Rev. Mod. Phys.* **40**, 677 (1968)
18. M. Imada, A. Fujimori, Y. Tokura, *Rev. Mod. Phys.* **70**, 1039 (1998)
19. M. Köhl, H. Moritz, T. Stöferle, K. Günter, T. Esslinger, *Phys. Rev. Lett.* **94**, 080403 (2005)
20. T. Esslinger, *Annu. Rev. Condens. Matter Phys.* **1**, 129 (2010)
21. U. Schneider, L. Hackermüller, S. Will, T. Best, I. Bloch, T.A. Costi, R.W. Helmes, D. Rasch, A. Rosch, *Science* **322**, 1520 (2008)
22. R. Jördens, N. Strohmaier, K. Günter, H. Moritz, T. Esslinger, *Nature* **455**, 204 (2008)
23. N. Gemelke, X. Zhang, C.L. Hung, C. Chin, *Nature* **460**, 995 (2009)
24. A. Itah, H. Veksler, O. Lahav, A. Blumkin, C. Moreno, C. Gordon, J. Steinhauer, *Phys. Rev. Lett.* **104**, 113001 (2010)
25. J.F. Sherson, C. Weitenberg, M. Endres, M. Cheneau, I. Bloch, S. Kuhr, *Nature* **467**, 68 (2010)
26. M. Endres, M. Cheneau, T. Fukuhara, C. Weitenberg, P. Schauß, C. Gross, L. Mazza, M.C. Bañuls, L. Pollet, I. Bloch et al., *Appl. Phys. B* **113**, 27 (2013)
27. D. Greif, M.F. Parsons, A. Mazurenko, C.S. Chiu, S. Blatt, F. Huber, G. Ji, M. Greiner, *Science* **351**, 953 (2016)
28. I.B. Mekhov, C. Maschler, H. Ritsch, *Phys. Rev. Lett.* **98**, 100402 (2007)
29. I.B. Mekhov, C. Maschler, H. Ritsch, *Nat. Phys.* **3**, 319 (2007)
30. I.B. Mekhov, C. Maschler, H. Ritsch, *Phys. Rev. A* **76**, 053618 (2007)
31. W. Chen, D. Meiser, P. Meystre, *Phys. Rev. A* **75**, 023812 (2007)
32. M.J. Bhaseen, M. Hohenadler, A.O. Silver, B.D. Simons, *Phys. Rev. Lett.* **102**, 135301 (2009)
33. H. Zoubi, H. Ritsch, *Phys. Rev. A* **80**, 053608 (2009)
34. A.O. Silver, M. Hohenadler, M.J. Bhaseen, B.D. Simons, *Phys. Rev. A* **81**, 023617 (2010)
35. S. Rajaram, N. Trivedi, *Phys. Rev. Lett.* **111**, 243603 (2013)
36. T.L. Dao, C. Kollath, I. Carusotto, M. Köhl, *Phys. Rev. A* **81**, 043626 (2010)
37. R. Landig, F. Brennecke, R. Mottl, T. Donner, T. Esslinger, *Nat. Commun.* **6**, 7046 (2015)
38. S.N. Sanders, F. Mintert, E.J. Heller, *Phys. Rev. Lett.* **105**, 035301 (2010)
39. K. Mayer, A. Rodriguez, A. Buchleitner, *Phys. Rev. A* **90**, 023629 (2014)
40. Q. Niu, I. Carusotto, A.B. Kuklov, *Phys. Rev. A* **73**, 053604 (2006)
41. N. ten Brinke, R. Schützhold, *Phys. Rev. A* **92**, 013617 (2015)
42. R.H. Dicke, *Phys. Rev.* **93**, 99 (1954)
43. N.E. Rehler, J.H. Eberly, *Phys. Rev. A* **3**, 1735 (1971)
44. H.J. Lipkin, in *Multiple Facets of Quantization and Supersymmetry*, edited by M. Olshanetsky, A. Vainshtein (World Scientific, Singapore, 2002), pp. 128–150
45. E. Akkermans, A. Gero, R. Kaiser, *Phys. Rev. Lett.* **101**, 103602 (2008)
46. R. Wiegner, J. von Zanthier, G.S. Agarwal, *Phys. Rev. A* **84**, 023805 (2011)
47. M.O. Scully, E.S. Fry, C.H.R. Ooi, K. Wódkiewicz, *Phys. Rev. Lett.* **96**, 010501 (2006)
48. M.O. Scully, *Laser Phys.* **17**, 635 (2007)
49. R.A. de Oliveira, M.S. Mendes, W.S. Martins, P.L. Saldanha, J.R. Tabosa, D. Felinto, *Phys. Rev. A* **90**, 023848 (2014)
50. S.L. Bromley, B. Zhu, M. Bishof, X. Zhang, T. Bothwell, J. Schachenmayer, T.L. Nicholson, R. Kaiser, S.F. Yelin, M.D. Lukin et al., *Nat. Commun.* **7**, 11039 (2016)

51. N. ten Brinke, R. Schützhold, D. Habs, Phys. Rev. A **87**, 053814 (2013)
52. R.J. Bettles, S.A. Gardiner, C.S. Adams, Phys. Rev. A **92**, 063822 (2015)
53. M.C. Gutzwiller, Phys. Rev. Lett. **10**, 159 (1963)
54. F. Queisser, K.V. Krutitsky, P. Navez, R. Schützhold, Phys. Rev. A **89**, 033616 (2014)
55. G.C. Wick, Phys. Rev. **80**, 268 (1950)
56. T.S. Evans, D.A. Steer, Nucl. Phys. B **474**, 481 (1996)
57. C. Halboth, W. Metzner, Z. Phys. B: Con. Mat. **102**, 501 (1997)
58. S. Inouye, M.R. Andrews, J. Stenger, H.J. Miesner, D.M. Stamper-Kurn, W. Ketterle, Nature **392**, 151 (1998)
59. W.B. Bridges, Appl. Phys. Lett. **4**, 128 (1964)
60. C.K.N. Patel, Phys. Rev. **136**, A1187 (1964)
61. D.M. Stamper-Kurn, M.R. Andrews, A.P. Chikkatur, S. Inouye, H.J. Miesner, J. Stenger, W. Ketterle, Phys. Rev. Lett. **80**, 2027 (1998)
62. T. Volz, N. Syassen, D.M. Bauer, E. Hansis, S. Durr, G. Rempe, Nat. Phys. **2**, 692 (2006)
63. S.A. Moses, J.P. Covey, M.T. Miecnikowski, B. Yan, B. Gadway, J. Ye, D.S. Jin, Science **350**, 659 (2015)
64. V.L. Berezinskii, JETP Lett. **20**, 287 (1974)
65. D.N. Zubarev, Sov. Phys. Usp. **3**, 320 (1960)